# Development of an Alternative Droop Strategy for Controlling Parallel Converters in Standalone DC Microgrid

PhD Oral Defence

By

Muamer Shebani

Supervisory Committee

Dr. Tariq Iqbal, Dr. John Quaicoe, Dr. Xiaodong Liang

Faculty of Engineering and Applied Science
Memorial University of Newfoundland
St. John’s, NL.

Dec 04, 2020

# OUT LINE

- Introduction
- Research Motivation
- Literature Review
- Alternative Droop strategy development
  - Circulating Current Minimization
  - Load Current Sharing Improvement
  - Voltage Regulation Improvement
- Dynamic Modeling, Simulation, and Control of a Residential Building Microgrid
  - Performance of the Solar-PV Array connected to the BESS and the Load Side Parallel-connected DC-DC converters
- Conclusion
  - Summary, Contributions, Future work

MEMORIAL

# INTRODUCTION:

- **Most of end residential users and office load are based on electronic DC loads.**
- **Integration of Renewable Energy sources into DC microgrid is more efficient compared to AC microgrid.**
- **Parallel-connection of low Converters versus single, high power and centralized power converter.**
- **Thermal Management, Reliability, Redundancy, Modularity, Maintainability, Size reduction.**

# INTRODUCTION:

- several schemes for controlling parallel-connected DC-DC converters have been proposed in the literature.

- Conventional droop control method are recognized with poor load sharing current, low voltage regulation and issue of circulating current.

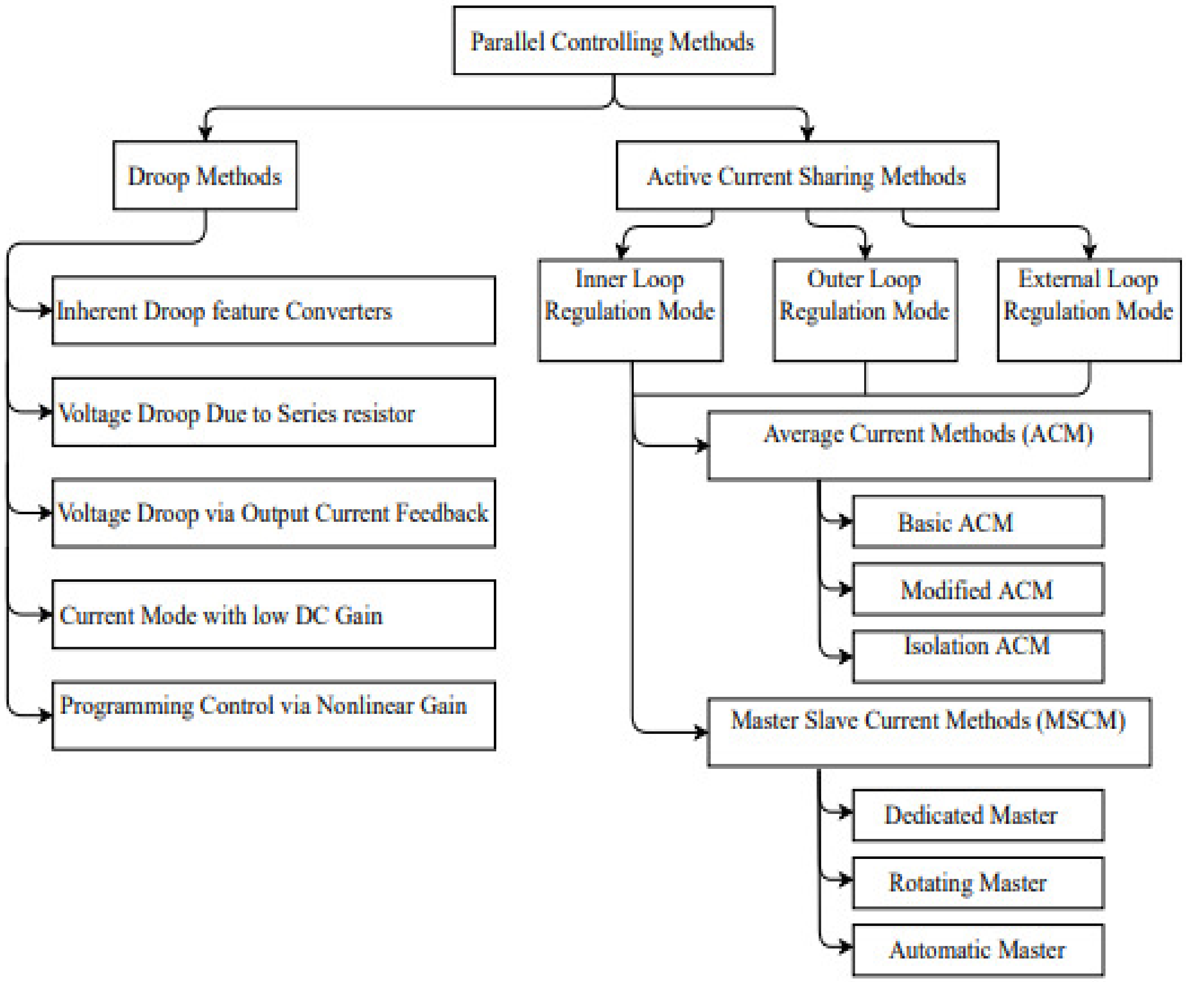


Fig. 1 Classification diagram for parallel controlling methods

# INTRODUCTION

- Parallel controlling schemes based the circuit theoretic viewpoint are classified into three types.
- First Type : Thevenin source
- Second Type: Thevenin source with many Norton sources in parallel
- Third Type : Norton sources in parallel only

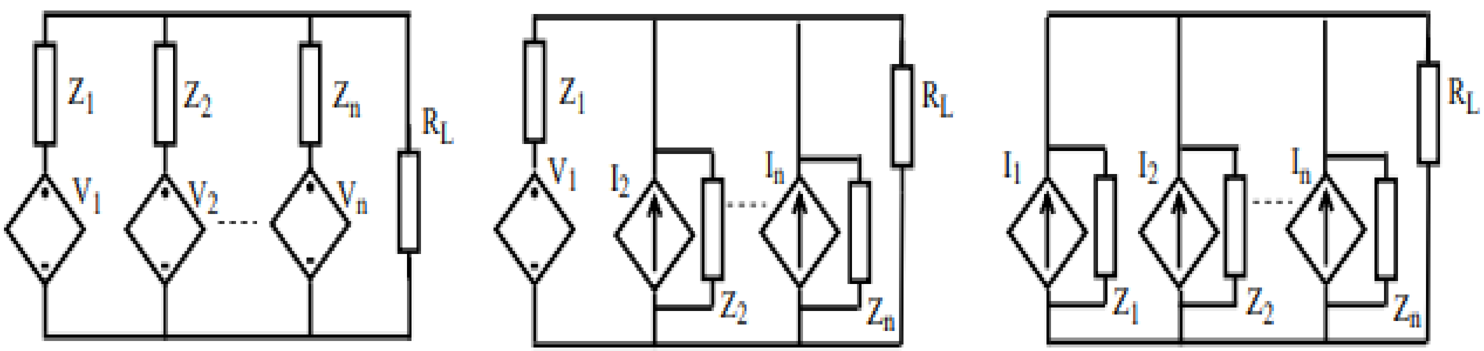


(a) First type (b) Second Type (c) Third Type

Fig. 2 Three configurations of paralleling converters

# RESEARCH MOTIVATION

- **Improved droop methods overcomes the drawbacks of conventional droop method by using communication network between parallel modules.**
- **The point of common coupling in DC microgrid makes the use of high-bandwidth communication network is costly and unsuitable.**
- **Conventional droop control method versus Improved droop methods ( The cost, accuracy, complexity, and reliability)**
- **Challenges associated with parallel-connected converters (circulating current, load current sharing and voltage regulation in case of the droop method)**

# LITERATURE REVIEW

- **Conventional Droop method: all parallel converters are presented by a voltage source in series with impedance (Thevenin source)**

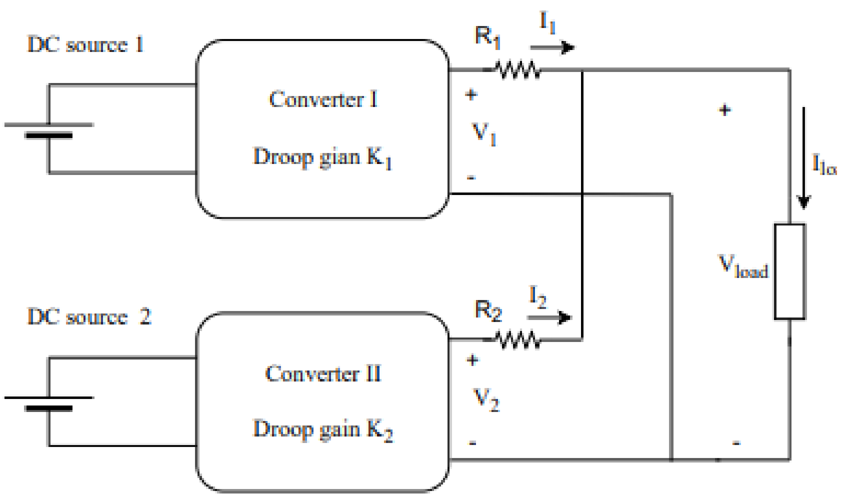


Fig. 3. Schematic diagram of the two parallel connected converters

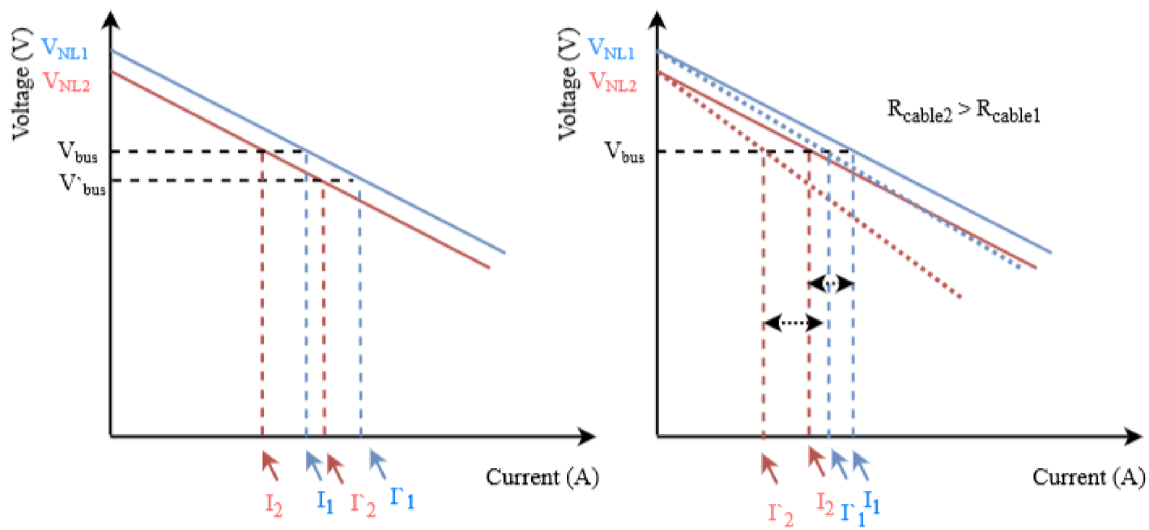


(a) difference in converters' parameters (b) difference in cable resistance

Fig. 4. Load regulation characteristic of the droop method with K1 and K2

# LITERATURE REVIEW

- **Meng et al. 2013, virtual resistance (VR) droop method is presented (A tertiary optimization control )**
- **Augustine et al. 2013, virtual resistance method is based on the droop index algorithm to improve the load current sharing**

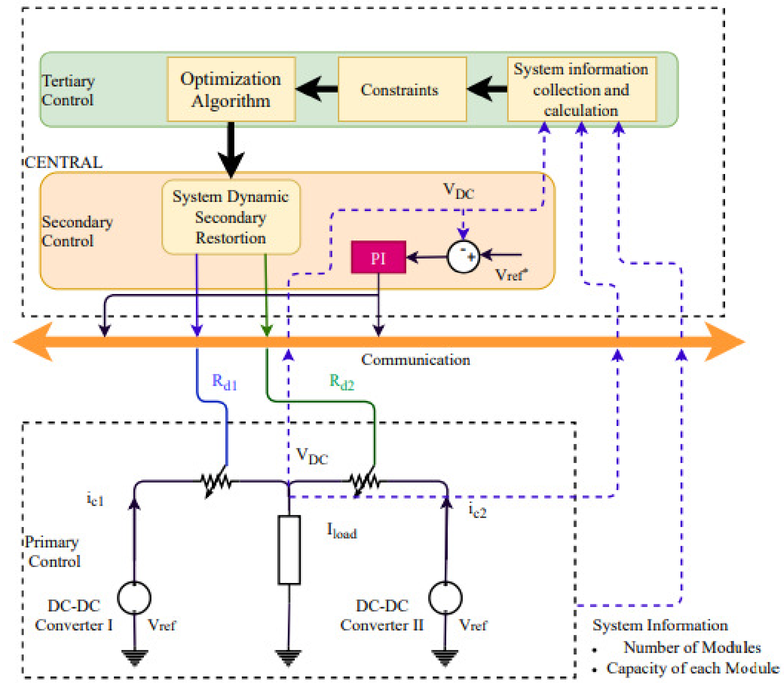


Fig. 5. Hierarchical Control in DC system

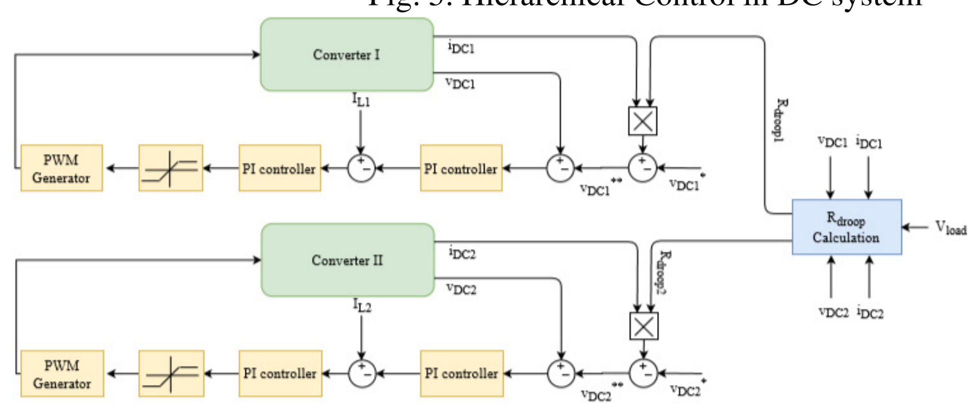


Fig. 6. Block diagram of parallel-connected converters with $R_{droop}$ calculation

# LITERATURE REVIEW

- **Anand et al. 2013, Distributed Control to Ensure Proportional Load Sharing and Improve Voltage Regulation in Low-Voltage DC Microgrid**
- **Augustine et al. 2015 Adaptive Droop Control Strategy for Load Sharing and Circulating Current Minimization in Low-Voltage Standalone DC Microgrid.**

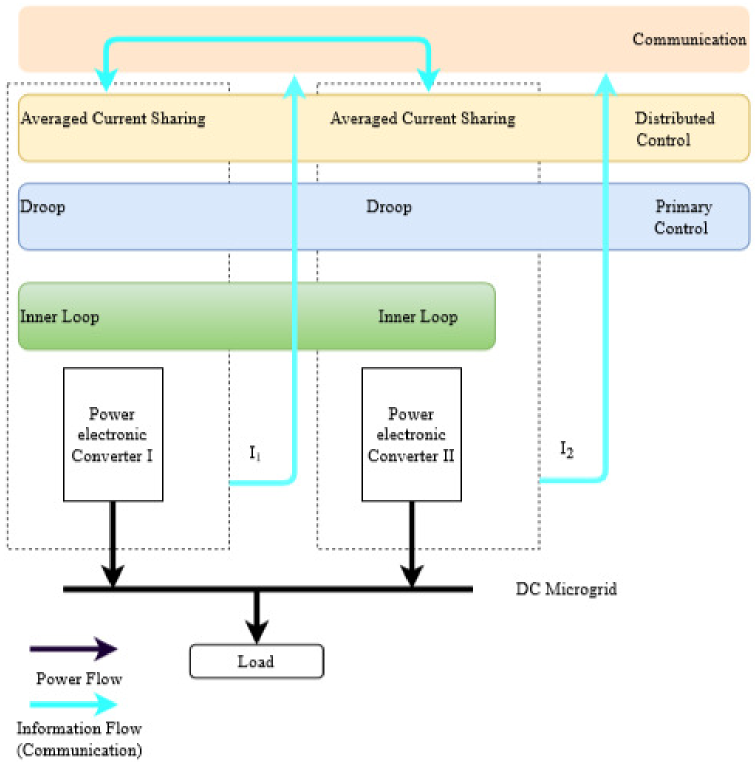


Fig. 7. Distributed control for parallel-connected DC-DC converters in a DC microgrid

# LITERATURE REVIEW

- **Lu et al. 2014, An Improved Droop Control Method for DC Microgrids Based on Low Bandwidth Communication With DC Bus Voltage Restoration and Enhanced Current Sharing Accuracy**

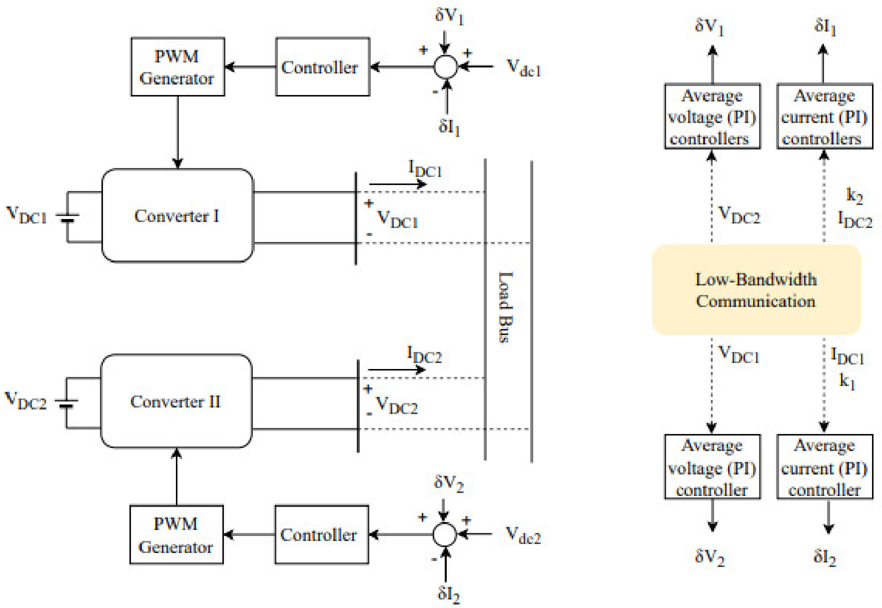


Fig. 8. Block diagram of the improved droop method based on the averaged voltage and current controller

# CIRCULATING CURRENT MINIMIZATION

- **The relationship between synchronous switching and circulating currents**
- **Different size of boost converters & Optimized controller**
- **Modified Droop Method Based on Master Current Control for Parallel-Connected DC-DC Boost Converters**
- **The parameters of the boost converter (50% mismatches in the power stage)**

TABLE 1. OPERATING VALUES FOR BOOST CONVERTERS

| Parameters | Converter I | Converter II |
|---|---|---|
| Switching frequency ***f*** | 25 KHz | 25 KHz |
| Inductance ***L*** | 23.712 mH | 11.856 mH |
| Capacitance ***C*** | 86.667 µF | 173.333 µF |
| Power ***P*** | 96 W | 192 W |

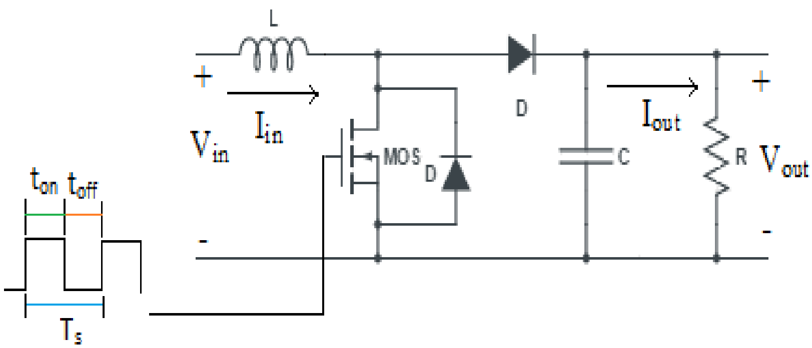


Fig. 9 DC-DC Boost Converter

# CIRCULATING CURRENT MINIMIZATION

- **Synchronous Switching Versus Asynchronous switching**

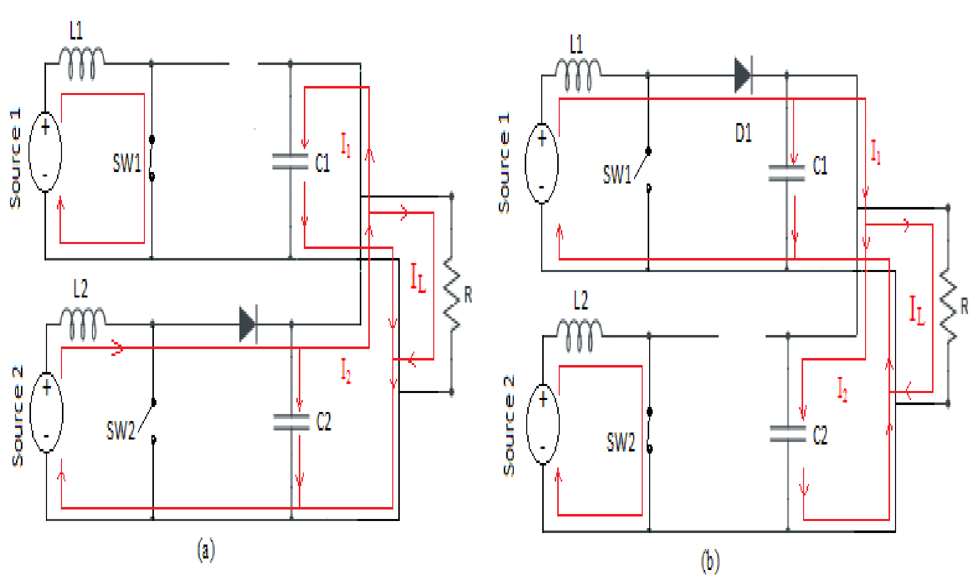


Fig. 10. Asynchronous switching of two parallel connected boost converters

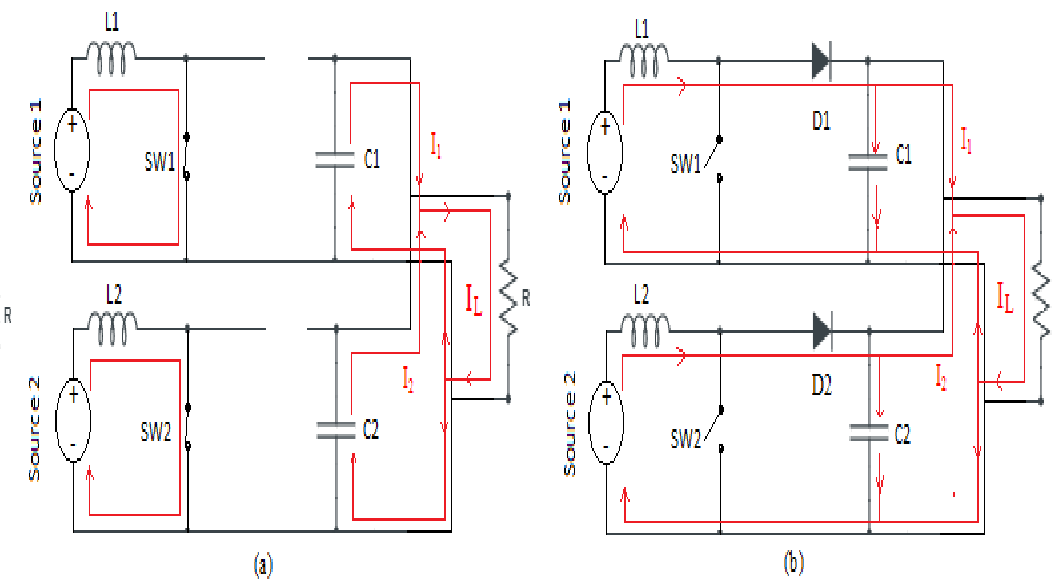


Fig. 11. Synchronous switching of two parallel connected boost converters

# CIRCULATING CURRENT MINIMIZATION

- **Load regulation characteristic of the droop method**
- **Boost converter droop gains (K1 & K2)**

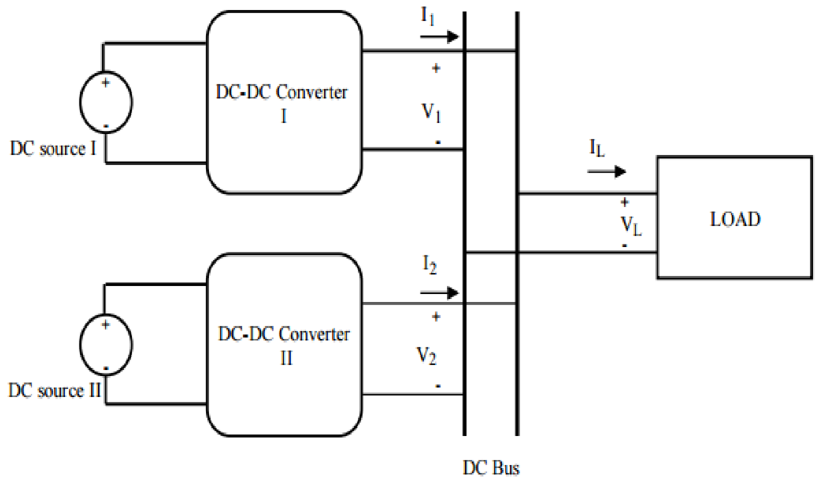


Fig. 12. Schematic diagram of the two parallel connected converters

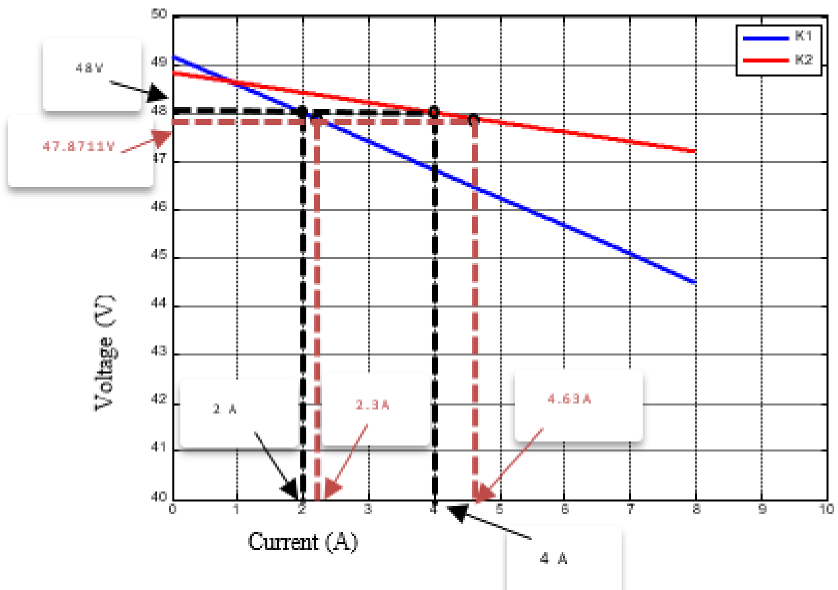


Fig. 13. Load regulation characteristic of the droop method with K1 and K2

# CIRCULATING CURRENT MINIMIZATION

- **State space averaging technique**
- **Design the PI controller for the inner and outer loops**
- **Optimized controller's design**

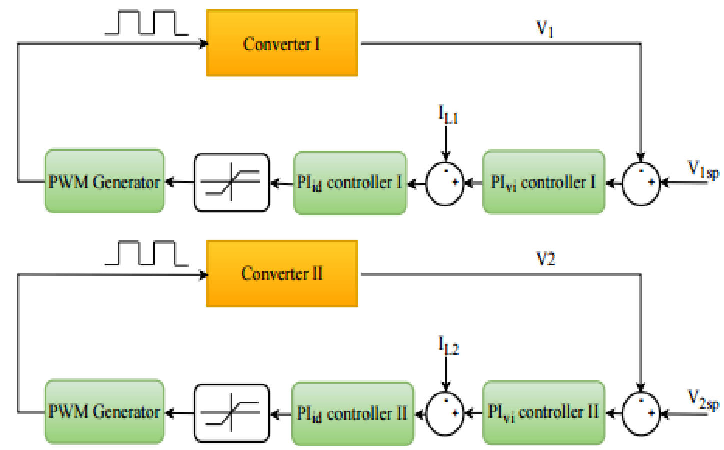


Fig. 14 Block diagram of two parallel-connected converters with their control loops

$$I_{L1synchronized} = (I_{L1} + I_{L2}) * (\frac{P_{converter\ I}}{P_{converter\ I} + P_{converter\ II}}) \quad (1)$$

$$I_{L2synchronized} = (I_{L1} + I_{L2}) * (\frac{P_{converter\ II}}{P_{converter\ I} + P_{converter\ II}}) \quad (2)$$

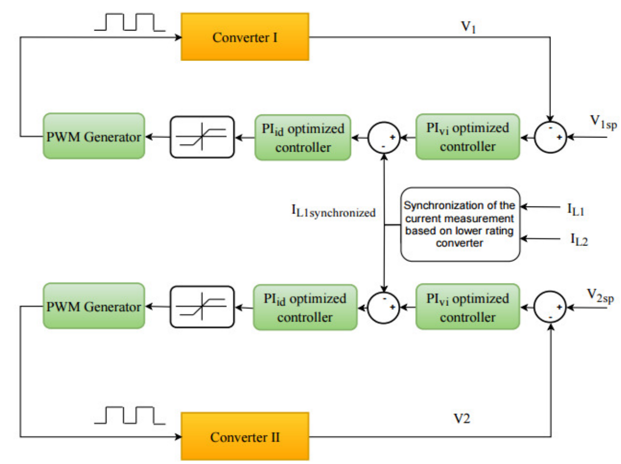


Fig. 15 Block diagram of two parallel-connected dc-dc boost converters with optimized control loops

# CIRCULATING CURRENT MINIMIZATION

- **Output currents (Non-optimized controller Vs  Optimized Controller)**

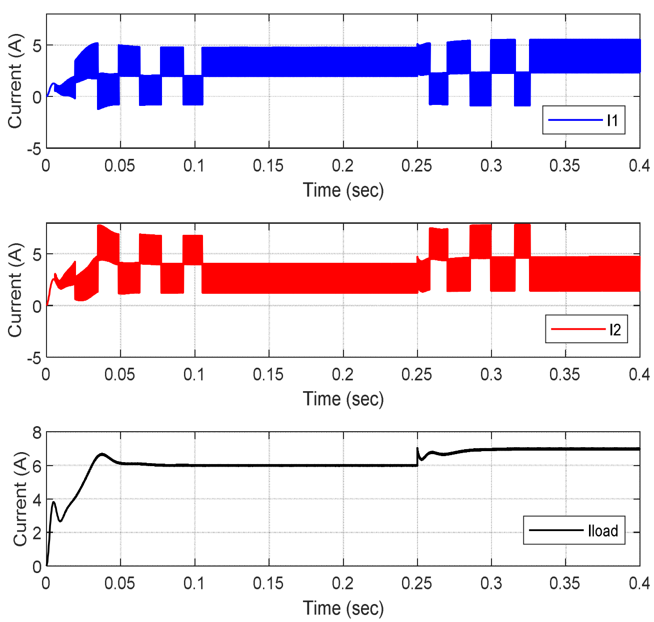


(a) Asynchronous switching

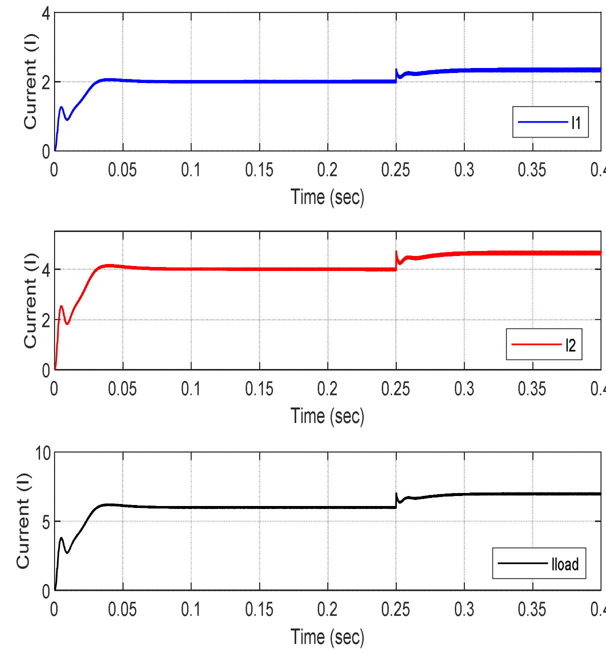


(b) Synchronous switching

Fig. 16  Output current waveforms for each converter and the total load current of the simulation results. (a) Asynchronous switching (b) Synchronous switching

# CIRCULATING CURRENT MINIMIZATION

- **Output currents for non-optimized controller VS Optimized Controller**

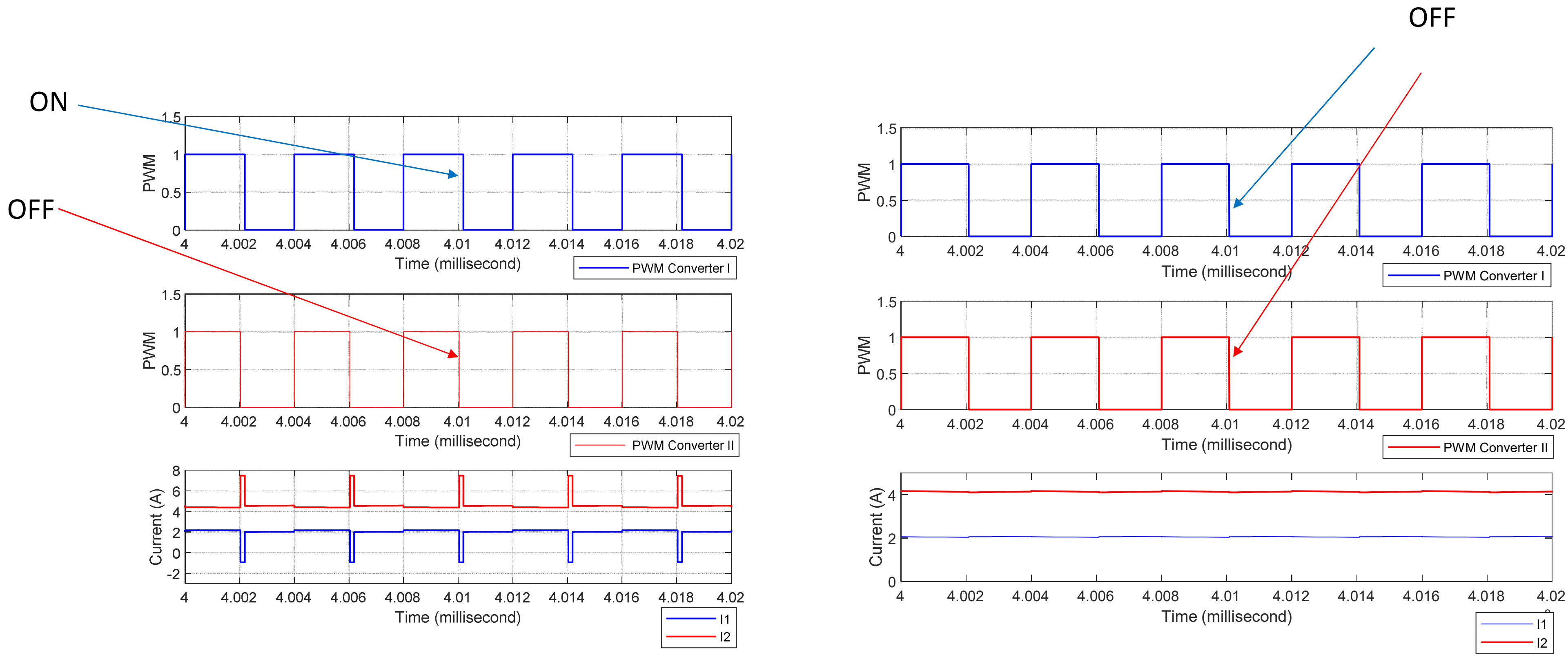


(a) Asynchronous switching

(b) Synchronous switching

Fig. 17 PWM with output current for both converters. (a) Asynchronized PWM (b) Synchronized PWM.

# CIRCULATING CURRENT MINIMIZATION

- **MATLAB/Simulink**
- **Two cases (Non-optimized and optimized controller)**

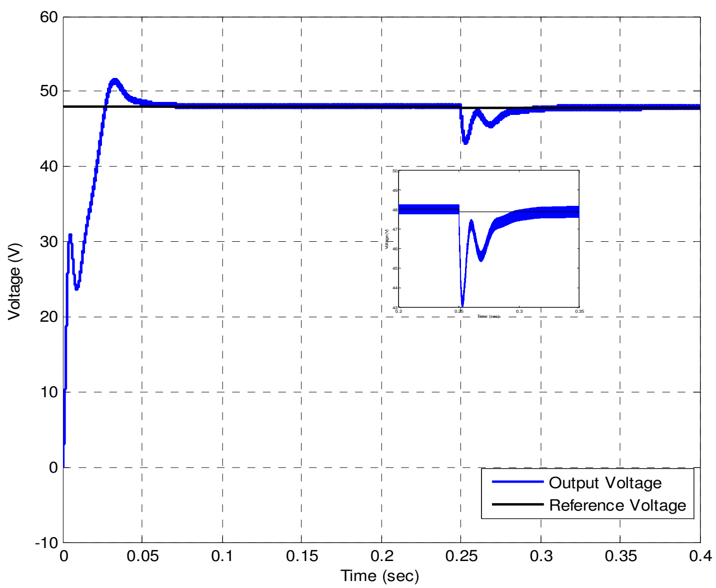


Fig. 18 Output Voltage with reference voltage for non-optimized controller

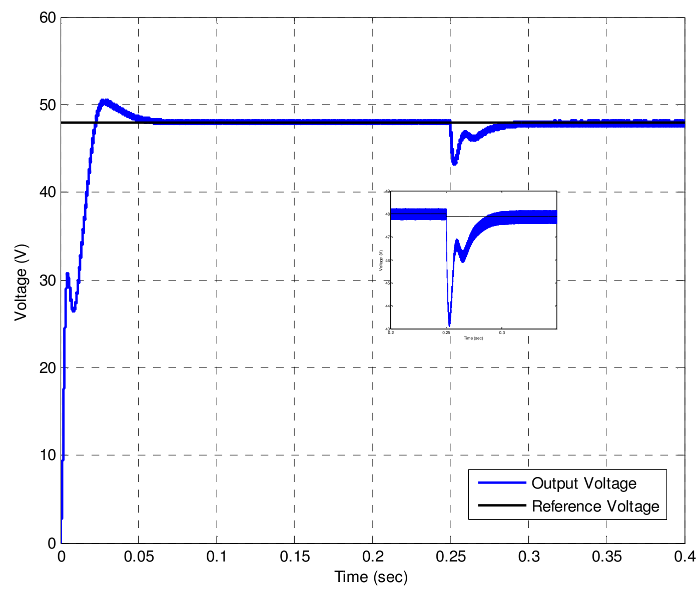


Fig. 19 Output voltage with reference voltage for optimized controller

# CIRCULATING CURRENT MINIMIZATION

- **Modified Droop Method Based on Master Current Control for Parallel-Connected DC-DC Boost Converters**

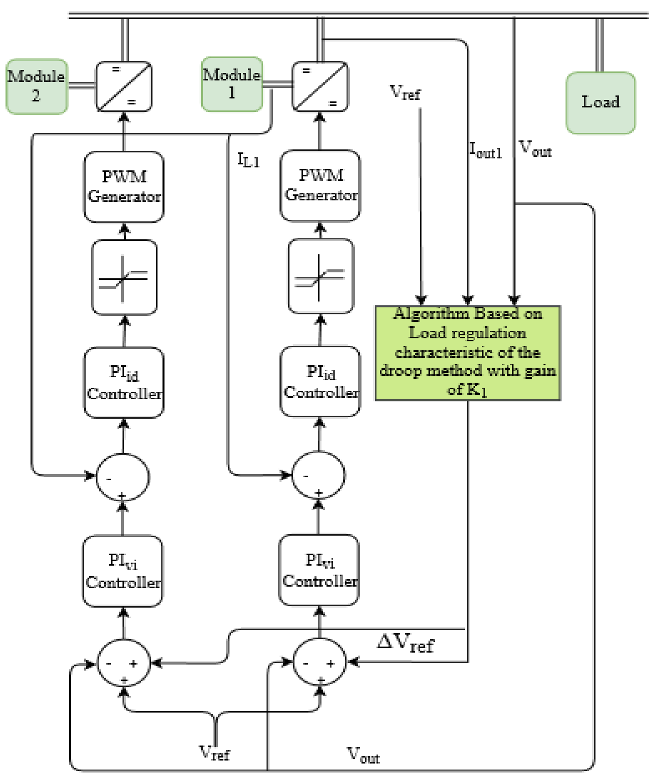


Fig. 20 Block diagram of two parallel-connected converters with their control loops and the proposed algorithm

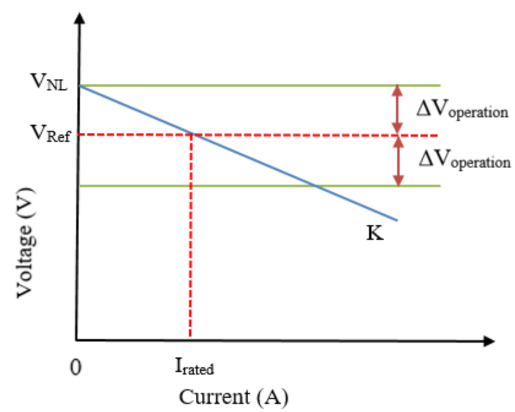


Fig. 21 Load regulation characteristic of the droop method with a gain of K

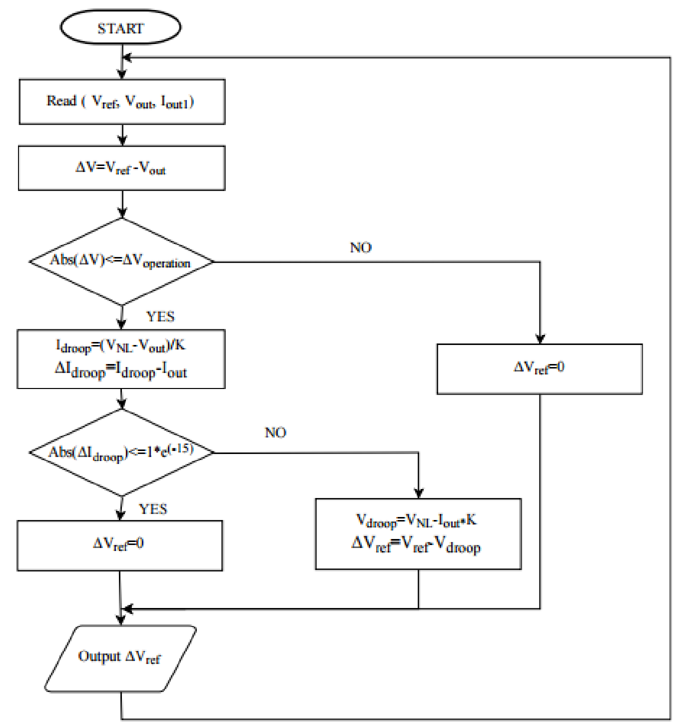


Fig. 22 Flow chart of the proposed algorithm

MEMORIAL

# CIRCULATING CURRENT MINIMIZATION

- **10% mismatch in the power stage**

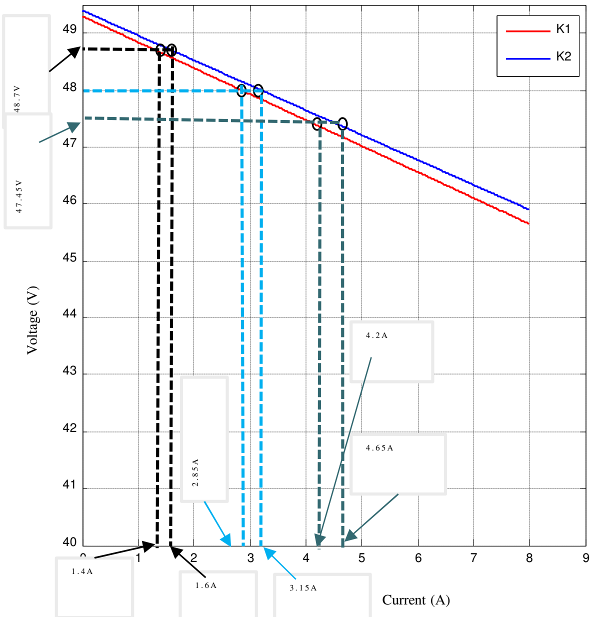


Fig. 23. Load regulation characteristic of the droop method with K1 and K2

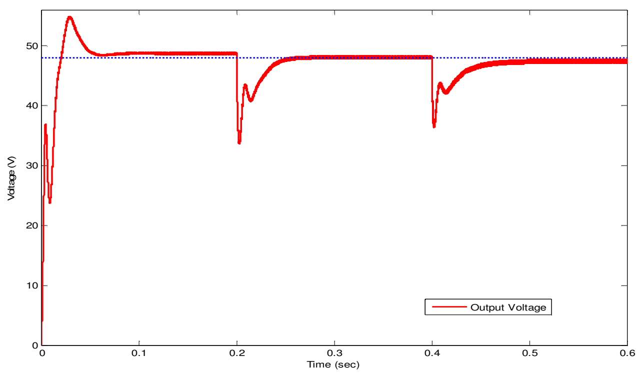


Fig. 24 Output voltage waveforms at each converter and the common DC bus

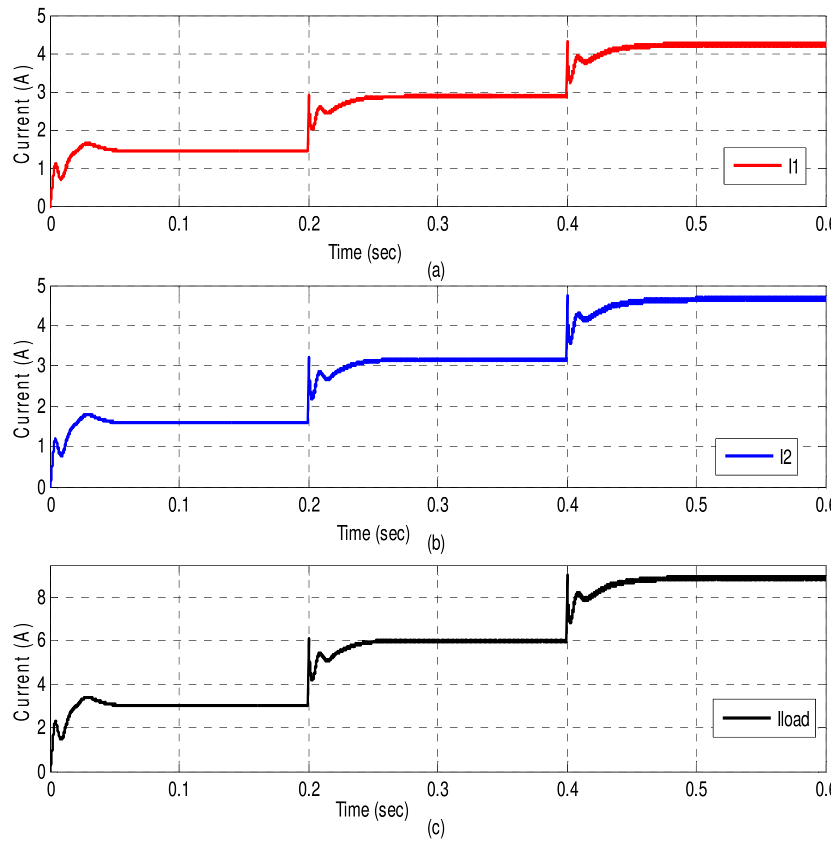


Fig. 25 The output current from the simulation results. (a) converter I output current (b) converter II output current (c) load current

# CIRCULATING CURRENT MINIMIZATION

- **20% mismatch in the power stage**

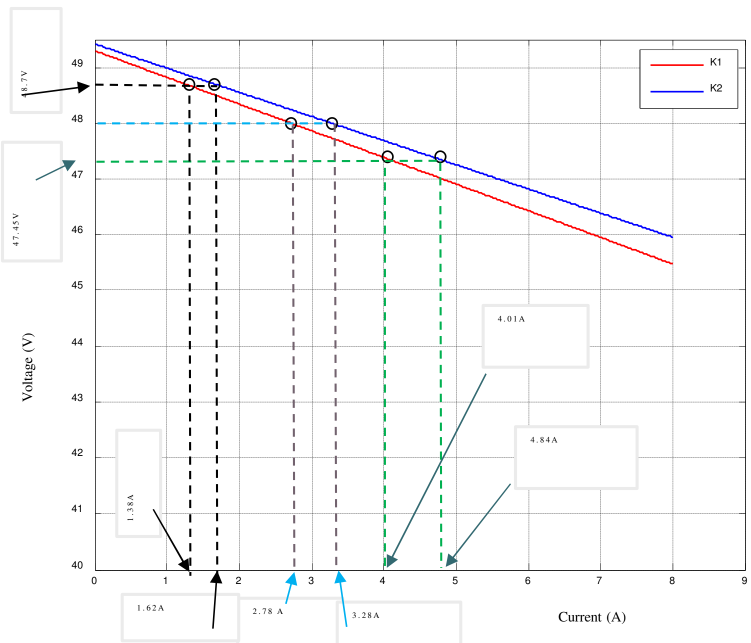


Fig. 26. Load regulation characteristic of the droop method with K1 and K2

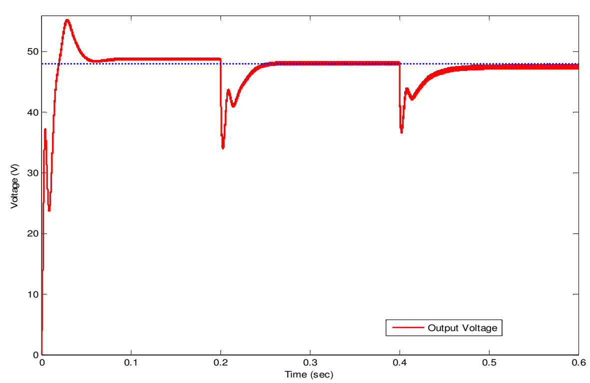


Fig. 27 Output voltage waveforms at each converter and the common DC bus

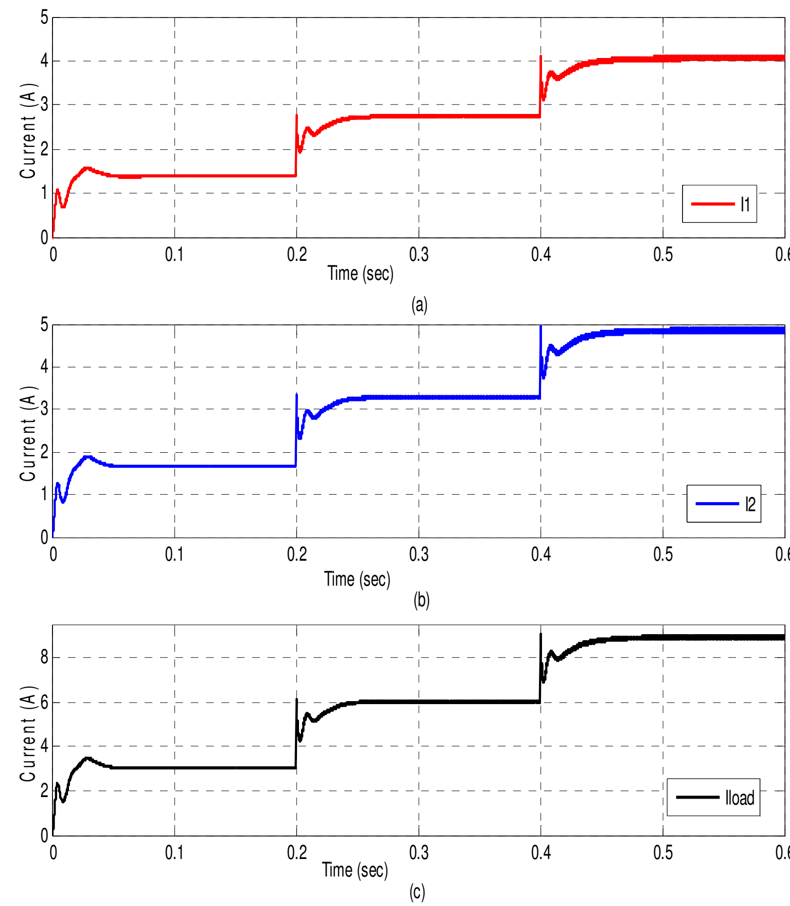


Fig. 28 The output current from the simulation results. (a) converter I output current (b) converter II output current (c) load current

# LOAD CURRENT SHARING IMPROVEMENT

- **Load regulation characteristic for the droop method**
- **Boost converter droop gains (K1 & K2)**

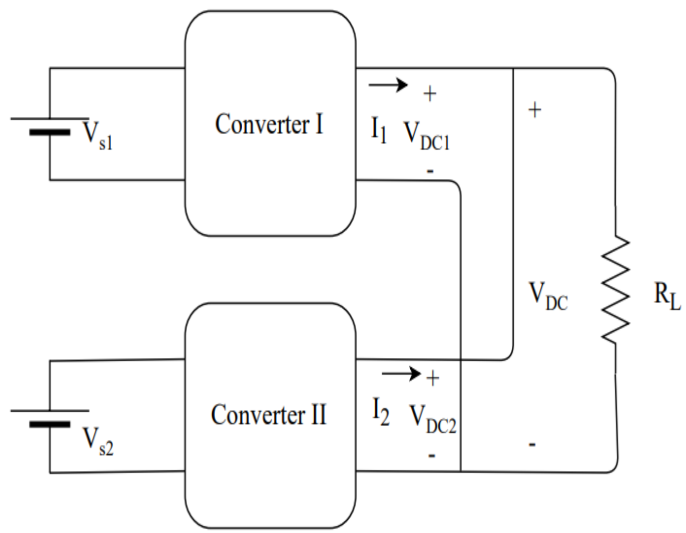


Fig. 29. Schematic diagram of the two parallel connected converters without cable resistance

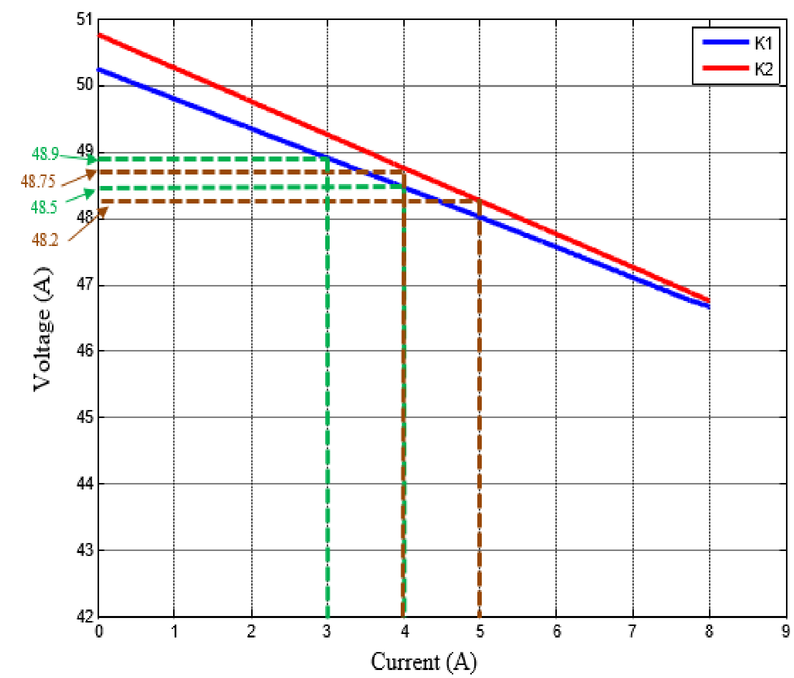


Fig. 30. Load regulation characteristic of the droop method with K1 and K2

$$V_n = V_{nNL} - K_n * I_n \qquad (3)$$

# LOAD CURRENT SHARING IMPROVEMENT

- **Modified Droop Control Method including cable Resistances**

$$V_L = V_{1NL} - (K_1 + R_{c1}) * I_1 \qquad (4)$$

$$V_L = V_{2NL} - (K_2 + R_{c2}) * I_2 \qquad (5)$$

$$V_L = R_L * (I_1 + I_2) \qquad (6)$$

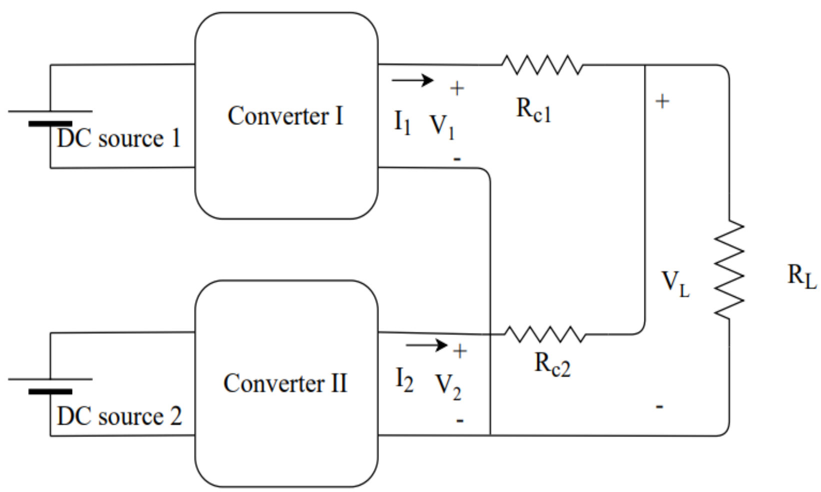


Fig. 31. Schematic diagram of the two parallel connected converters with cable resistance

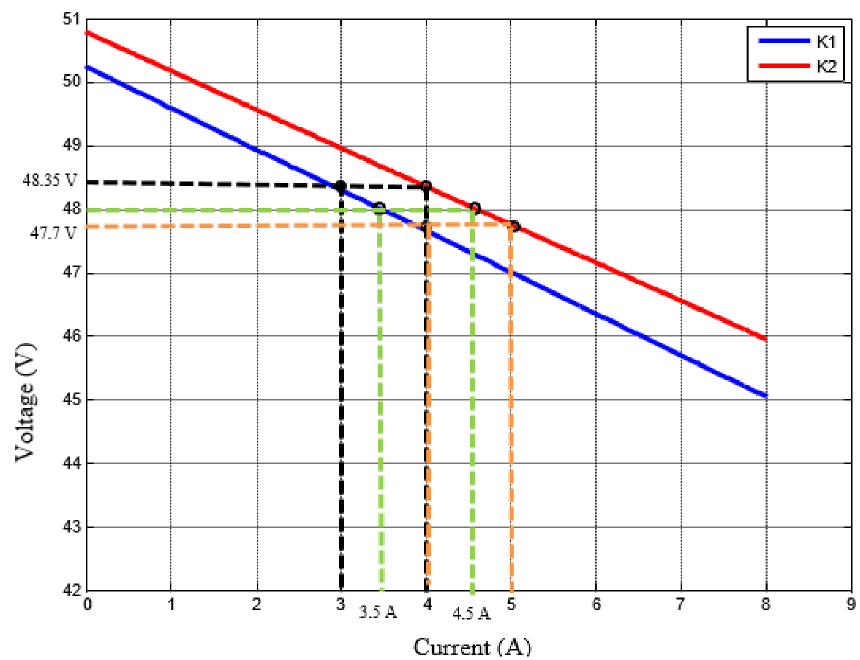


Fig. 32. Modified load regulation characteristics for both converters

# LOAD CURRENT SHARING IMPROVEMENT

- **Rearranging Eq (4), (5), and (6), we can write the following linear equations**

$$(R_L + R_{c1}) * I_1 + R_L * I_2 = V_{1NL} \qquad (7)$$

$$R_L * I_1 + (R_L + R_{c2}) * I_2 = V_{2NL} \qquad (8)$$

- **Solving Eq (7), and (8), we can calculate the theatrical values for I1 and I2 as**

$$I_1 = \frac{V_{2NL}/R_L - V_{1NL}/R_L^2 * (K_2 + R_{c2} + R_L)}{1 - 1/R_L^2 * (K_1 + R_{c1} + R_L) * (K_2 + R_{c2} + R_L)} \qquad (9)$$

$$V_L(theoretical) = V_{1NL} - (K_1 + R_{c1}) * I_1$$

$$Vset1(theoretical) = V_L(theoretical) + I_1 * R_{c1}$$

$$I_2 = \frac{V_{1NL}/R_L - V_{2NL}/R_L^2 * (K_1 + R_{c1} + R_L)}{1 - 1/R_L^2 * (K_1 + R_{c1} + R_L) * (K_2 + R_{c2} + R_L)} \qquad (10)$$

$$V_L(theoretical) = V_{2NL} - (K_2 + R_{c2}) * I_2$$

$$Vset2(theoretical) = V_L(theoretical) + I_2 * R_{c2}$$

MEMORIAL

# LOAD CURRENT SHARING IMPROVEMENT

- **Generalizing the concept of the modified droop control method for n parallel connected converters**

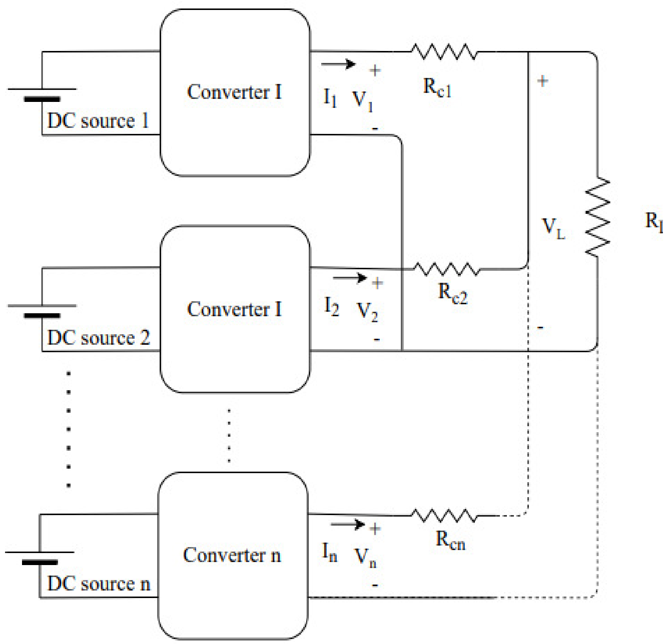


Fig. 33. n parallel converters connected to DC load through different values of cable resistances

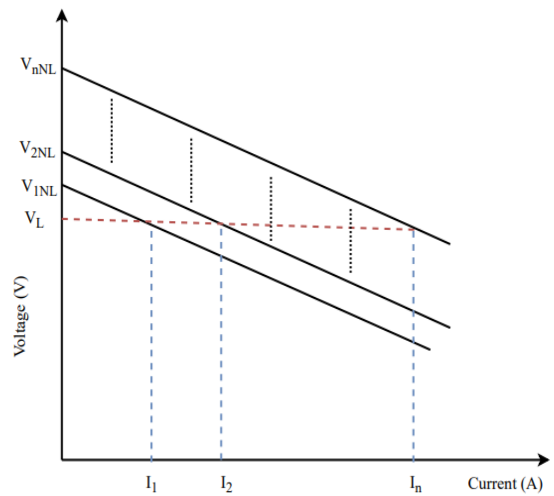


Fig. 34. Load regulation characteristics for n parallel converters taking into account the cable resistances

$$\begin{aligned} V_L &= V_{1NL} - (K_1 + R_{c1}) * I_1 \\ V_L &= V_{2NL} - (K_2 + R_{c2}) * I_2 \\ &\vdots \\ V_L &= V_{nNL} - (K_n + R_{cn}) * I_n \end{aligned} \qquad (11)$$

$$V_L = R_L * (I_1 + I_2 + \cdots + I_n) \qquad (12)$$

$$RK_{coefficeint} * \mathrm{I} = V_{NL} \qquad (13)$$

# LOAD CURRENT SHARING IMPROVEMENT

- **RKcoefficieint, I, and VNL matrices are given by**

$$RK_{coefficeint} = \begin{bmatrix} (K_1 + R_{c1} + R_L) & R_L & \cdots & R_L \\ R_L & (K_2 + R_{c2} + R_L) & \cdots & R_L \\ \vdots & \vdots & \ddots & \vdots \\ R_L & R_L & \ldots(K_n + R_{cn} + R_L) \end{bmatrix} \quad (14)$$

$$I = \begin{bmatrix} I_1 \\ I_2 \\ \vdots \\ I_{\mathrm{n}} \end{bmatrix} \quad (15) \qquad V_{NL} = \begin{bmatrix} V_{1NL} \\ V_{2NL} \\ \vdots \\ V_{\mathrm{n}NL} \end{bmatrix} \quad (16)$$

$$\mathrm{I} = (RK_{coefficeint})^{-1} * V_{NL} \quad (17)$$

$$V_L(theoretical) = V_{\mathrm{i}NL} - (K_i + R_{ci}) * I_{\mathrm{i}} \quad (18)$$

$$Vseti(theoretical) = V_L(theoretical) + I_{\mathrm{i}} * R_{ci} \quad (19)$$

# LOAD CURRENT SHARING IMPROVEMENT

- **Simulation Results and Discussion**
- **10% mismatches in power stage**
- **Different cable resistances**
- **Rc1=0.1 ohm and Rc2=0.2 ohm**

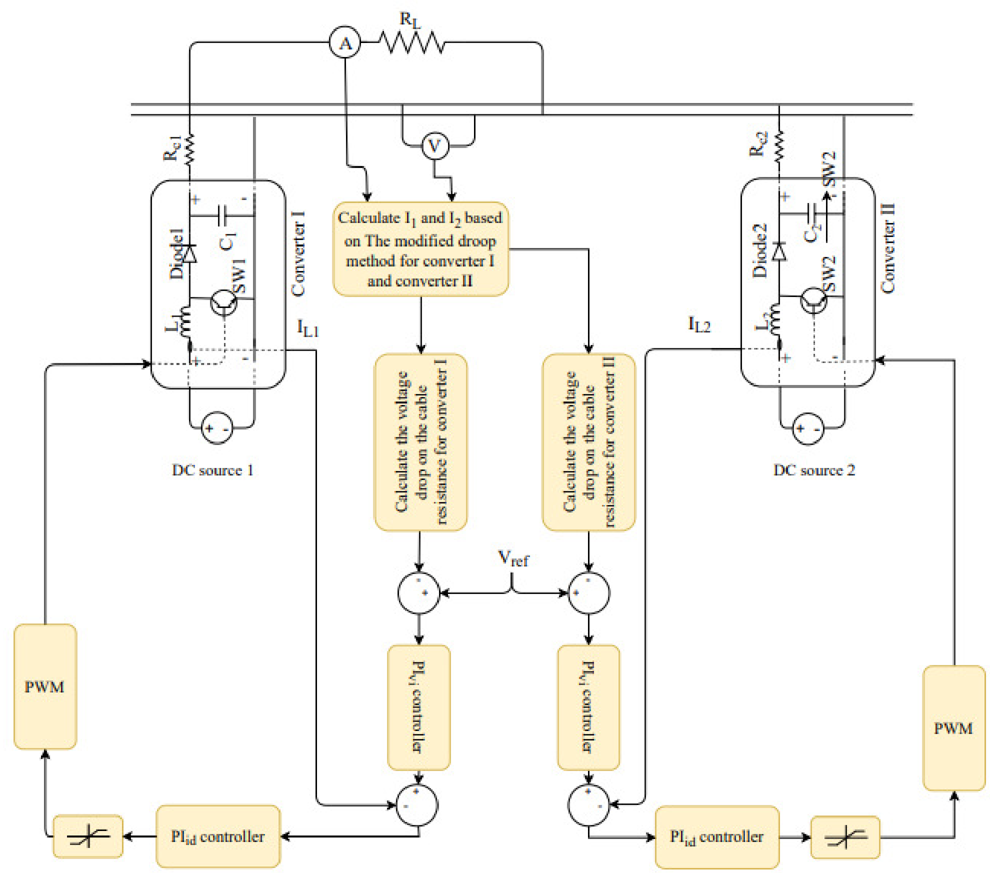


Fig. 35 Block diagram of the two parallel-connected converters showing their control loops

# LOAD CURRENT SHARING IMPROVEMENT

- **Output voltage waveforms at each converter and the common DC bus**

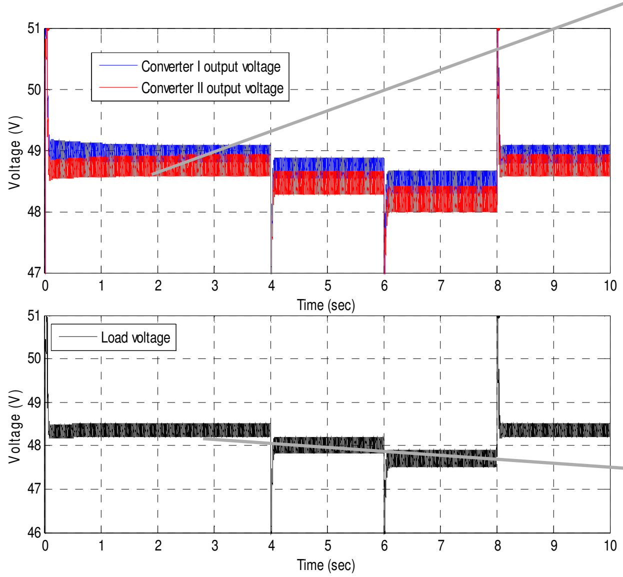


Fig. 36 Output voltage waveforms at each converter and the common DC bus

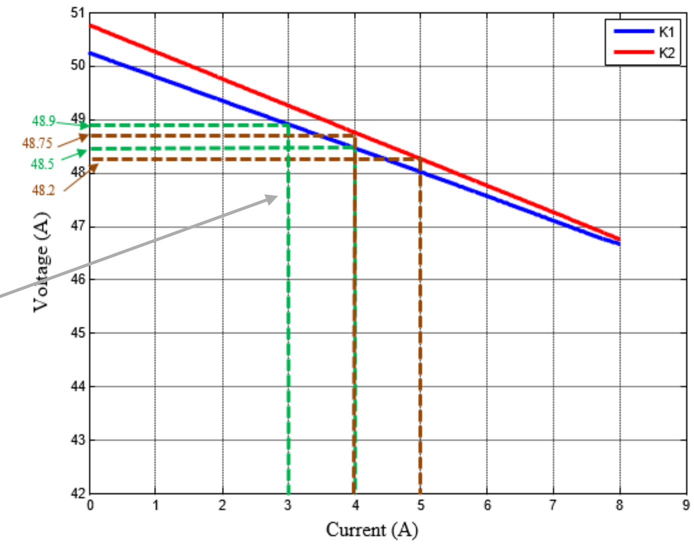


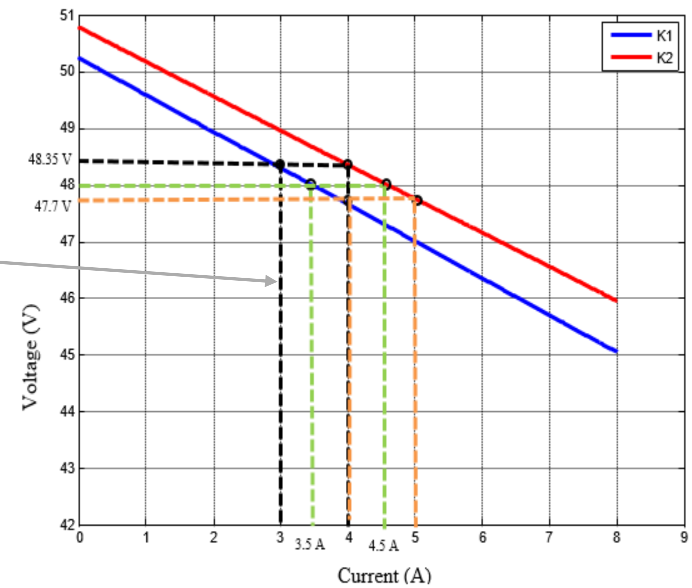

# LOAD CURRENT SHARING IMPROVEMENT

- **Output waveforms for the current of converter I, II and the load current**

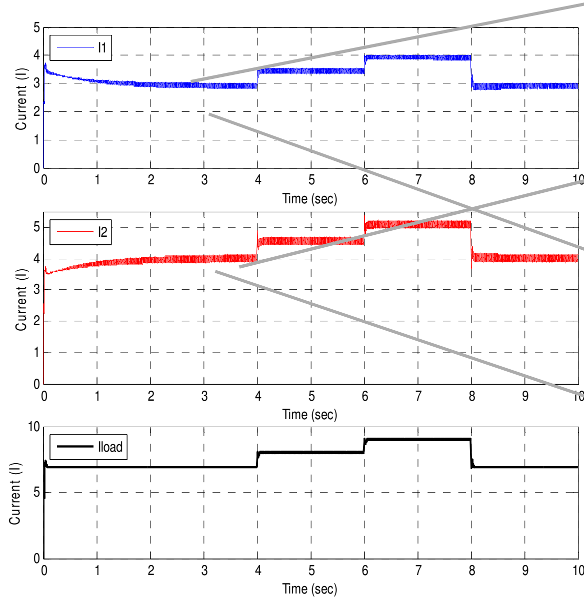


Fig. 37 Output waveforms for the current of converter I and II and the load current

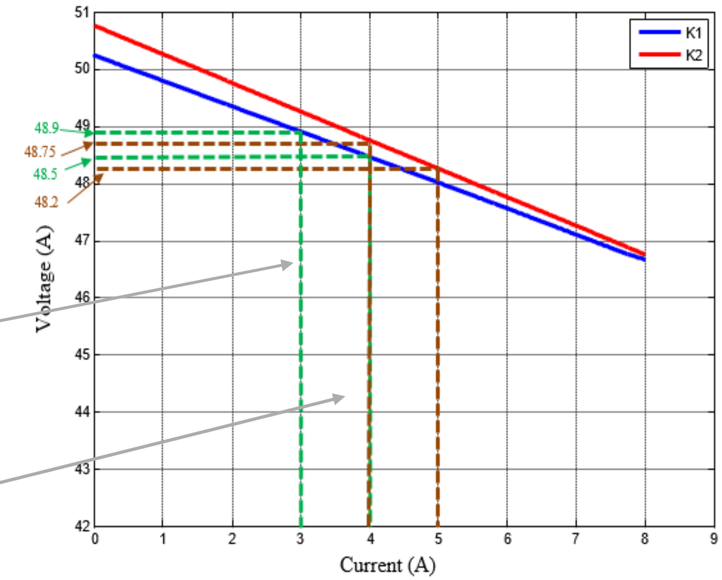


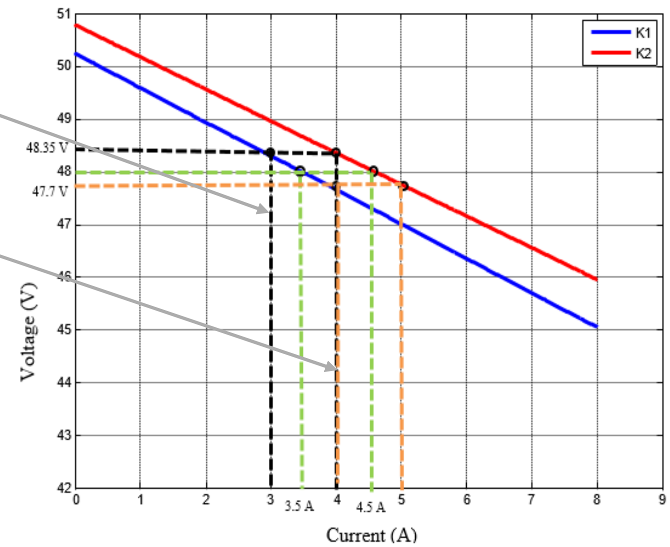

# LOAD CURRENT SHARING IMPROVEMENT

- **The Effect of Cable Resistance Based on Modified Droop Method**

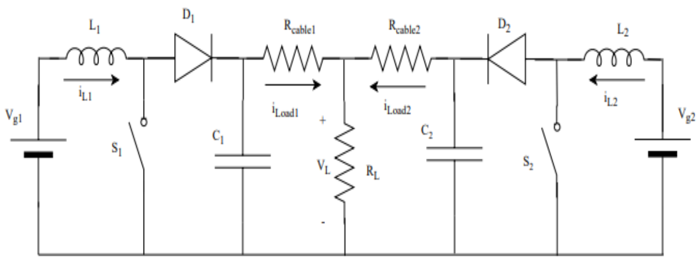


Fig. 38 Circuit diagram of two parallel-connected boost

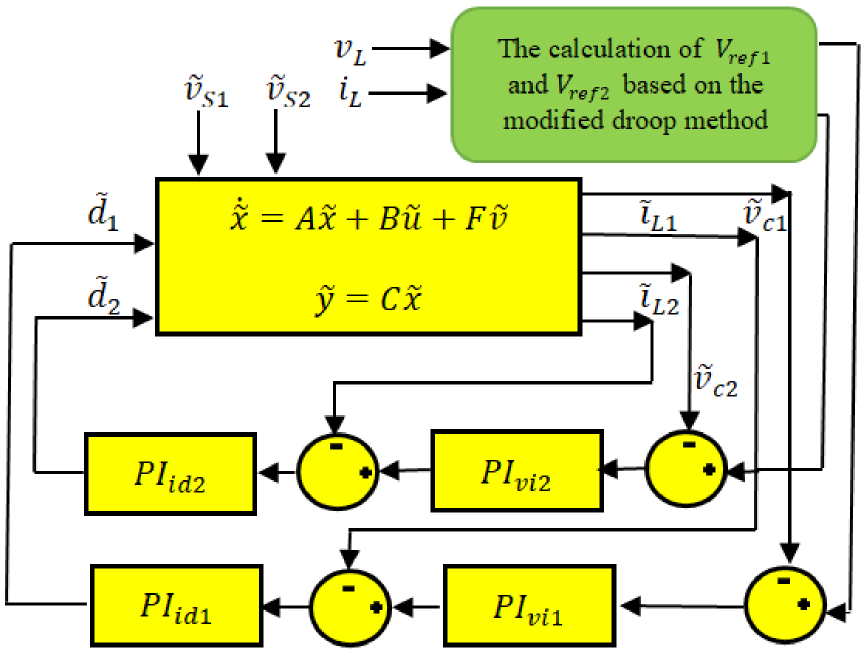


Fig. 39 Block diagram of the model representing the dynamics of the two parallel-connected boost converters system

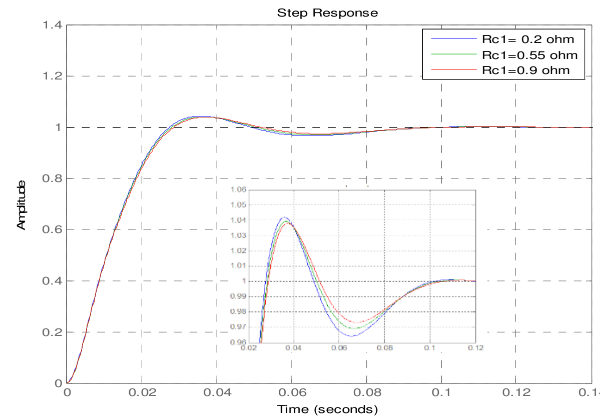


Fig. 40 Step response for $\tilde{v}_{c1}$ to $\tilde{d}_1$ with different values of $Rcable_1$

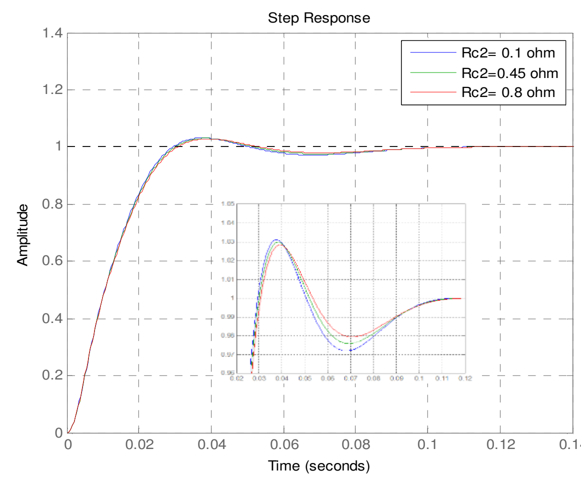


Fig. 41 Step response for $\tilde{v}_{c2}$ to $\tilde{d}_2$ with different values of $Rcable_2$

MEMORIAL

# LOAD CURRENT SHARING IMPROVEMENT

- **The Effect of Cable Resistance Based on Modified Droop Method**

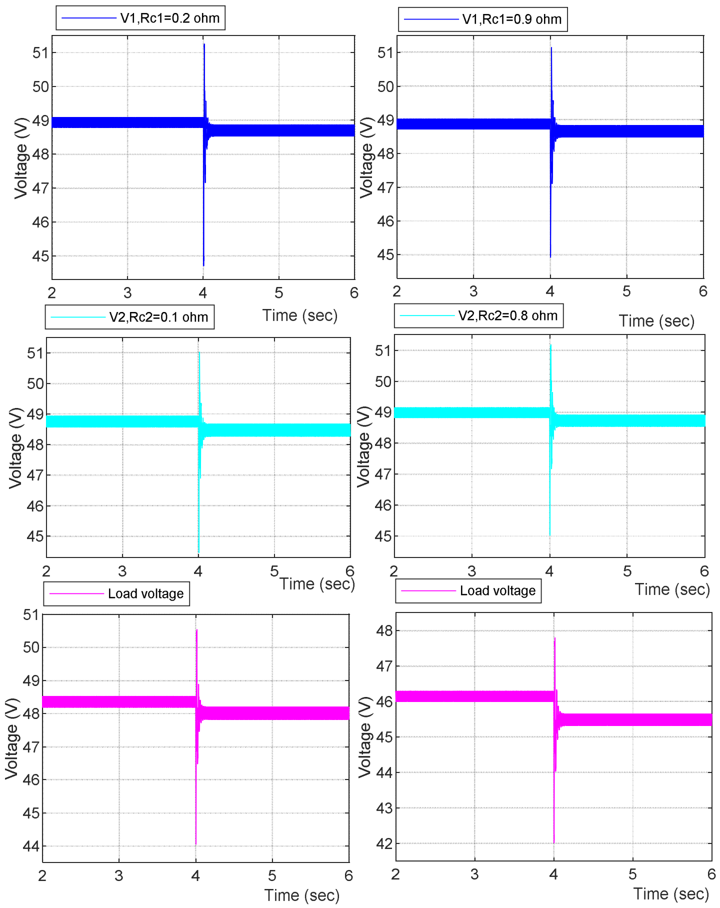


Fig. 42 Output voltage waveforms of the transient response for a step increase in the load

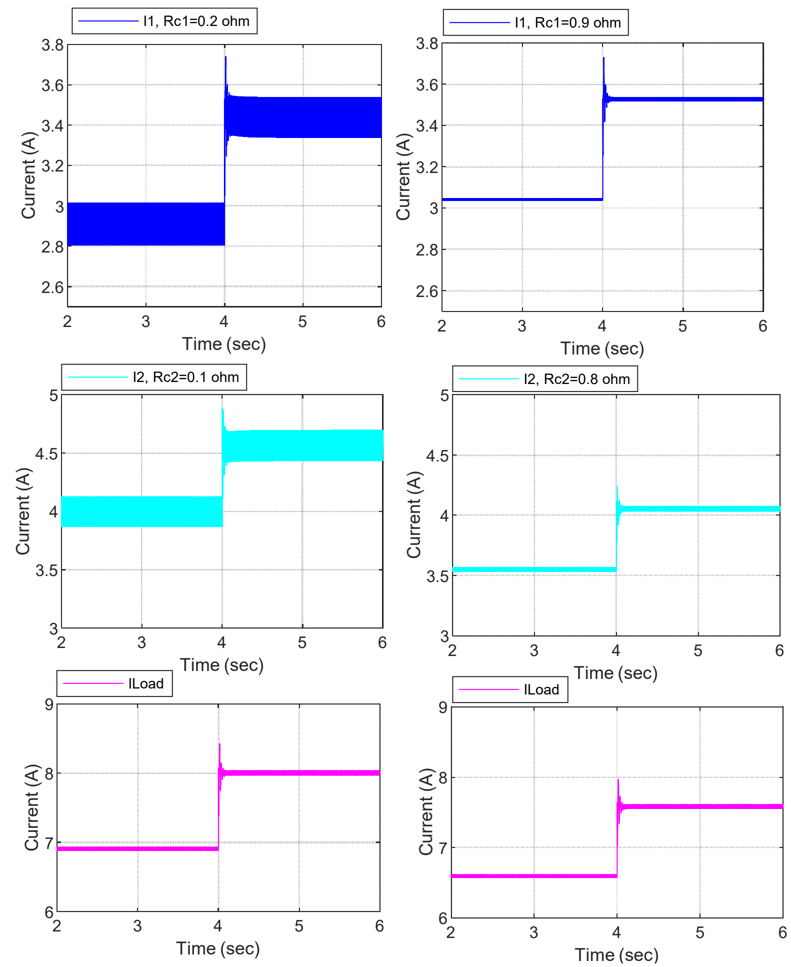


Fig. 43 Output current waveforms of the transient response for a step increase in the load

MEMORIAL

# LOAD CURRENT SHARING IMPROVEMENT

- **Control Algorithm for Equal Current Sharing between Parallel-connected Converters**

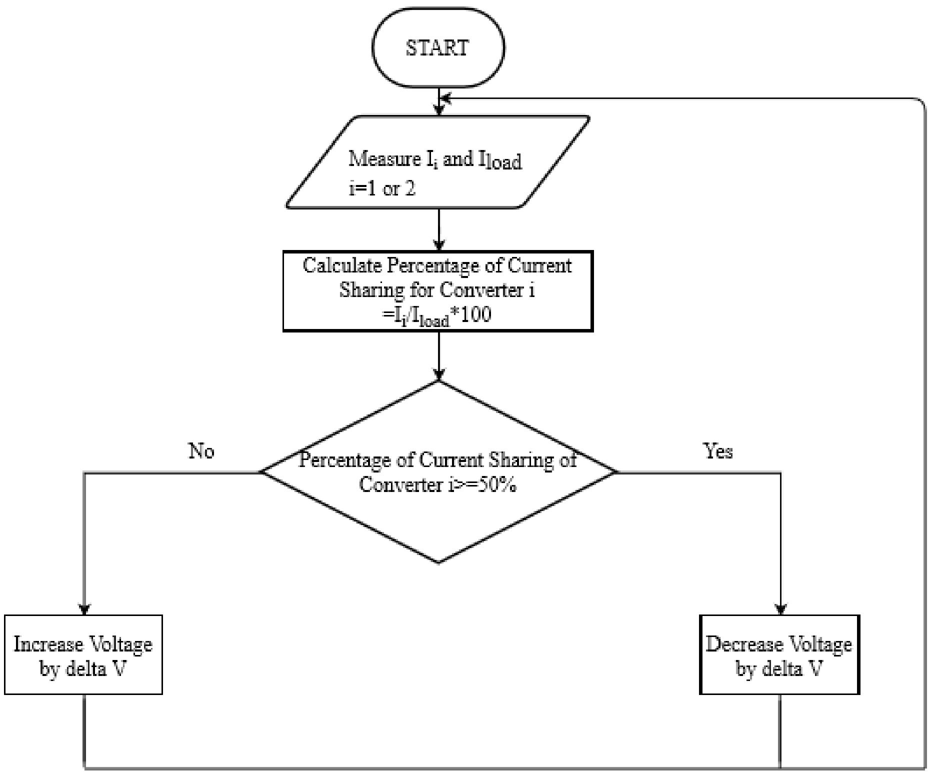


Fig. 44 Flow chart of the proposed algorithm

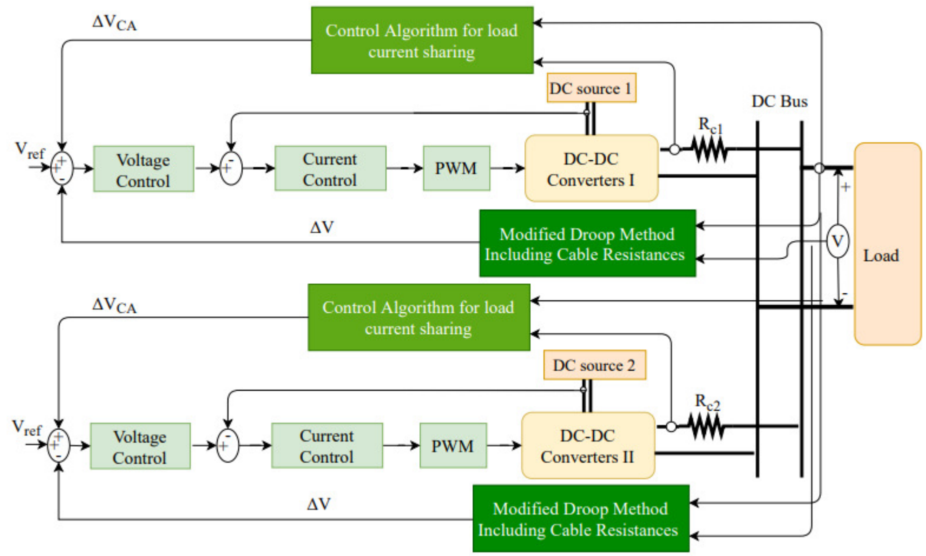


Fig. 45 Block diagram of the two parallel-connected converters with the proposed

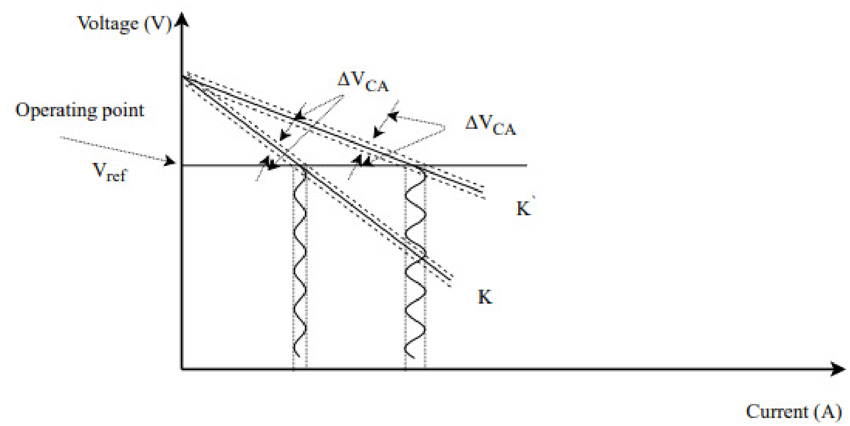


Fig. 46 Oscillatory current around the desired operating point for two droop gains with $K > K^{`}$

# LOAD CURRENT SHARING IMPROVEMENT

- **Simulation Results**

**Modified droop control Method VS Control Algorithm**

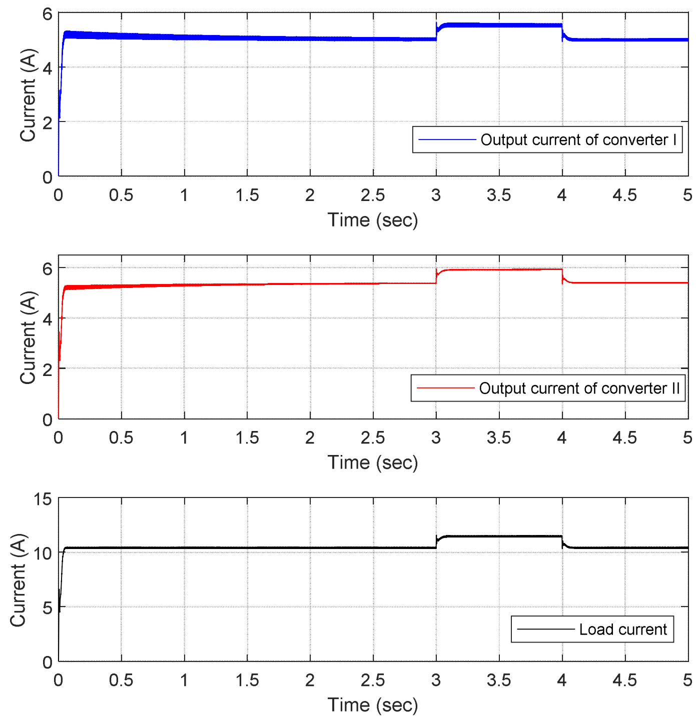


Fig. 47 Output waveforms of the converters' current and the load current (Modified droop Method)

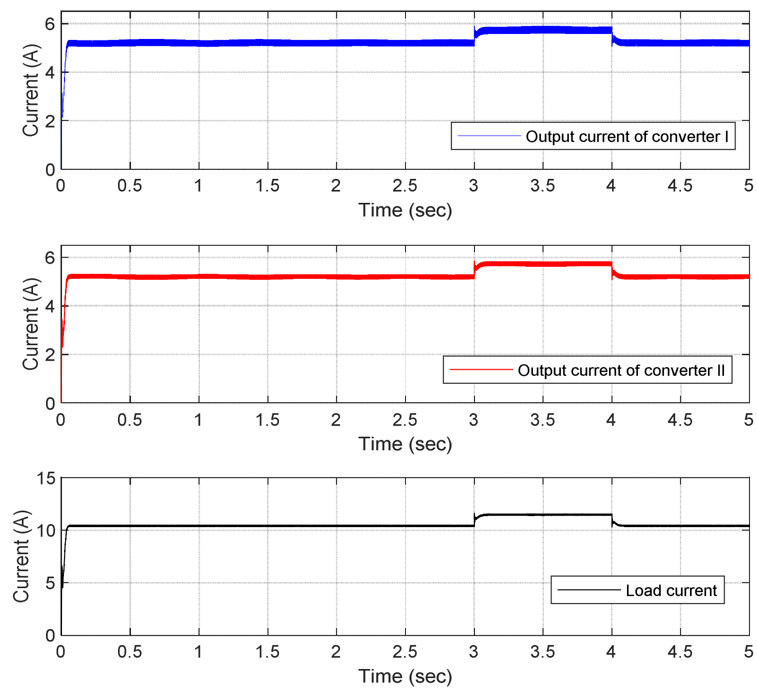


Fig. 48 Output waveforms of the converters' current and the load current (Control Algorithm)

# LOAD CURRENT SHARING IMPROVEMENT

- **Control Algorithm for Equal Current Sharing between Parallel-connected Converters**

## Steady state values

Table 2 Load current sharing for parallel-connected converters and the percentage of current deviation

| Case | Time | Converter I | Converter II | Load current | Percentage of current deviation % |
|---|---|---|---|---|---|
| Equal Cable Resistance | 0-3 sec | 5.0 A | 5.4 A | 10.4 A | 3.9 % |
| | 3-4 sec | 5.5 A | 5.9 A | 11.4 A | 3.5 % |
| | 4-5 sec | 5.0 A | 5.4 A | 10.4 A | 3.9 % |
| Control Algorithm | 0-3 sec | 5.2 A | 5.2 A | 10.4 A | 0 % |
| | 3-4 sec | 5.7 A | 5.7 A | 11.4 A | 0 % |
| | 4-5 sec | 5.2 A | 5.2 A | 10.4 A | 0 % |

# LOAD CURRENT SHARING IMPROVEMENT

- **Small Scale for experimental validation (MATLAB/Simulink Simulation)**

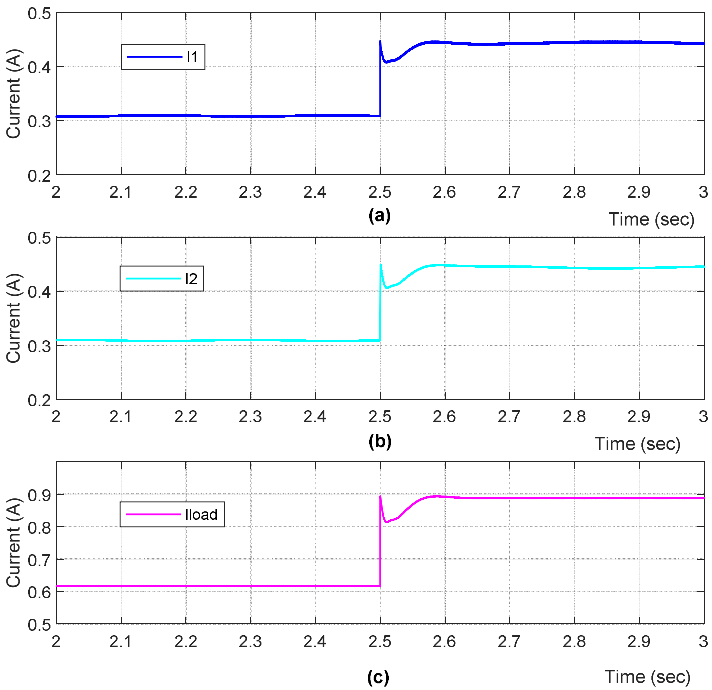


Fig. 49 Simulation results for the proposed algorithm with an increase in the load. (a) Output current of converter I. (b) Output current of converter II. (c) Total load current

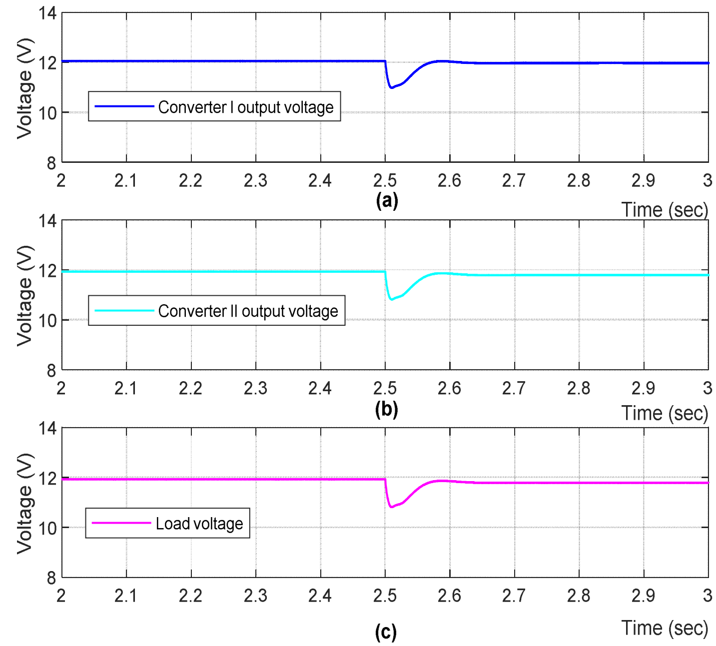


Fig. 50 Simulation results for the proposed algorithm with an increase in the load. (a) The output voltage of converter I. (b) The output voltage of converter II. (c) The voltage at the common DC bus

Table 3 Steady state values

| Time (sec) | $V_{out1}$ (V) | $V_{out2}$ (V) | $V_{load}$ (V) | $I_1$ (A) | $I_2$ (A) | $I_{load}$ (A) | $\Delta I$ % current sharing differences |
|---|---|---|---|---|---|---|---|
| 0-2.5 | 12.05 | 12.05 | 11.93 | 0.308 | 0.308 | 0.61 | 0 |
| 2.5-5 | 11.97 | 11.96 | 11.79 | 0.44 | 0.44 | 0.88 | 0 |

# LOAD CURRENT SHARING IMPROVEMENT

- **Control Algorithm for Equal Current Sharing between Parallel-connected Converters**

  - **experimental validation**
  - **dSPACE 1104 in real-time**

TABLE 4. OPERATING VALUES FOR BOOST CONVERTERS

| Parameters | Converter I | Converter II |
|---|---|---|
| Switching frequency ***f*** | 25 KHz | 25 KHz |
| Inductance ***L*** | 12.49 mH | 12.75 mH |
| Capacitance ***C*** | 570 µF | 620 µF |
| Voltage V | 6-12 V | 6-12 V |

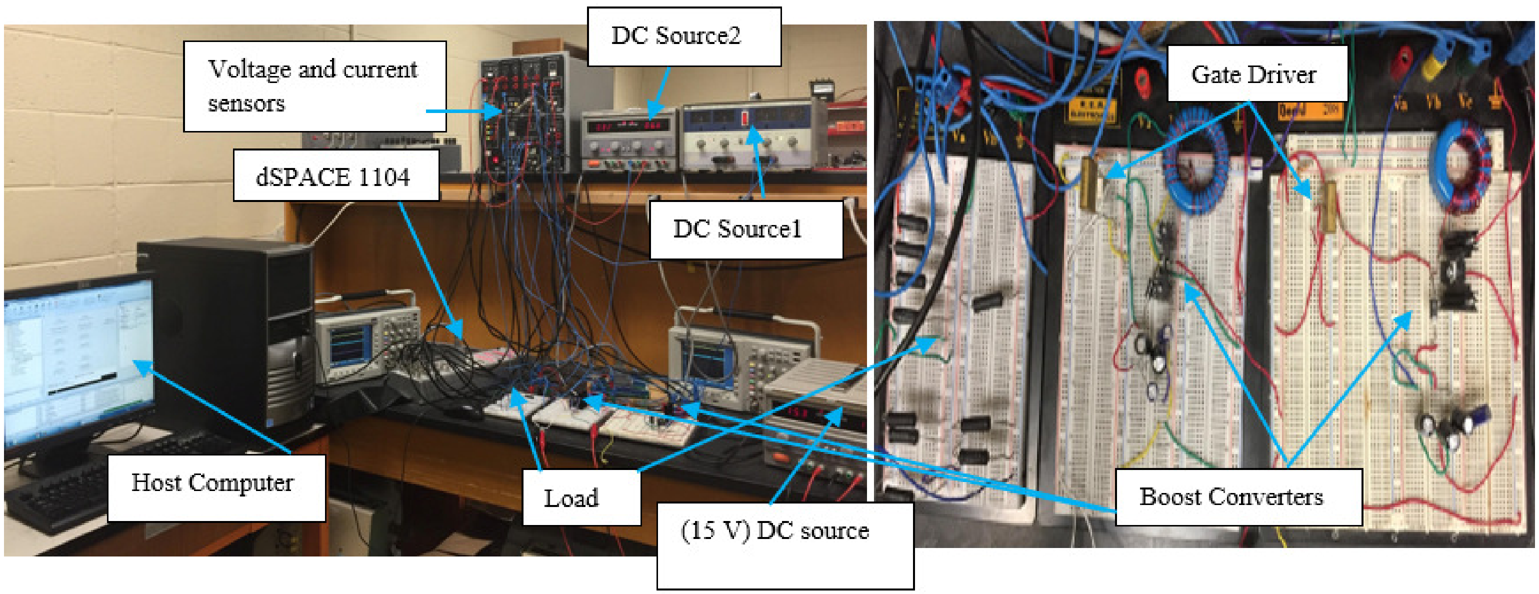


Fig. 51 Photograph of the experimental setups

# LOAD CURRENT SHARING IMPROVEMENT

- **Control Algorithm for Equal Current Sharing between Parallel-connected Converters**

  - **Experimental Results**

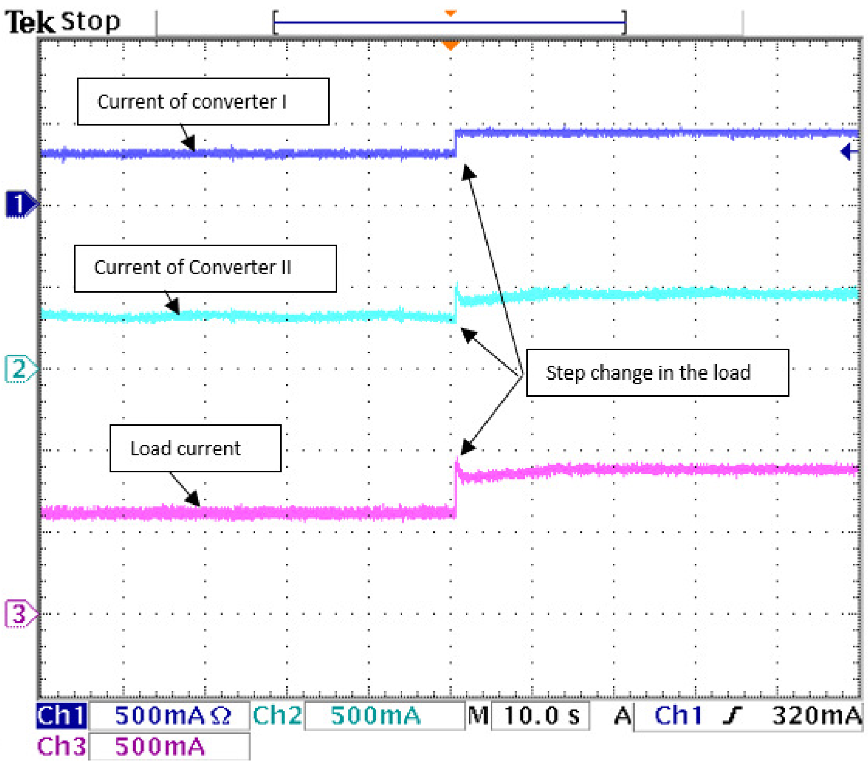


Fig. 52 Output current waveforms for each converter and the total load current of the proposed algorithm

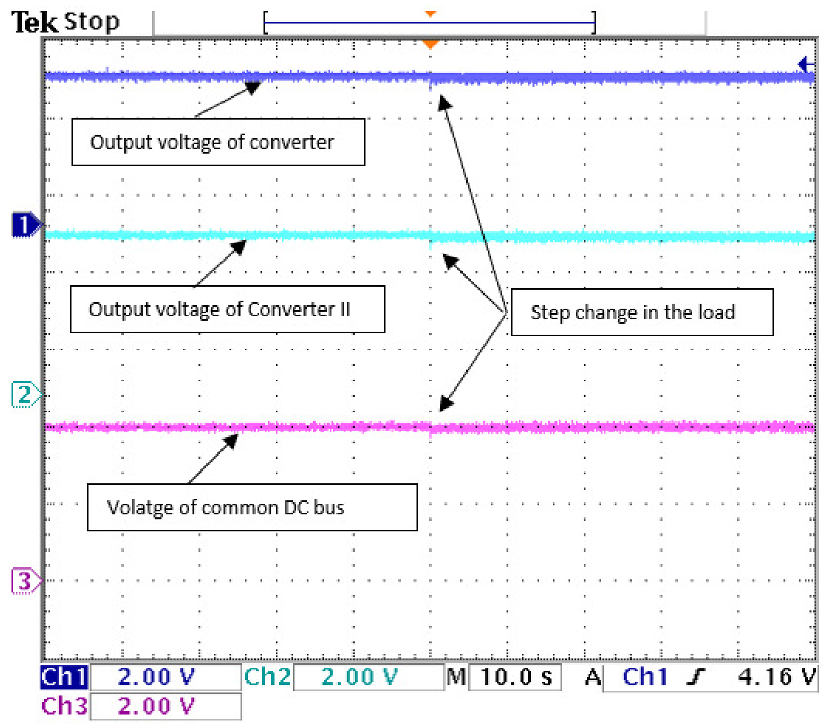


Fig. 53 Output voltage waveforms at each converter and the common DC bus of the proposed algorithm

# IMPROVED DROOP CONTROL METHOD

- **Virtually Droop Gain (VDG)**

$$V_L = V_{1NL} - (K_1 + R_{c1} + K_{v1}) * I_1 \qquad (20)$$

$$V_L = V_{2NL} - (K_2 + R_{c2} + K_{v2}) * I_2 \qquad (21)$$

$$V_L = R_L * (I_1 + I_2) \qquad (22)$$

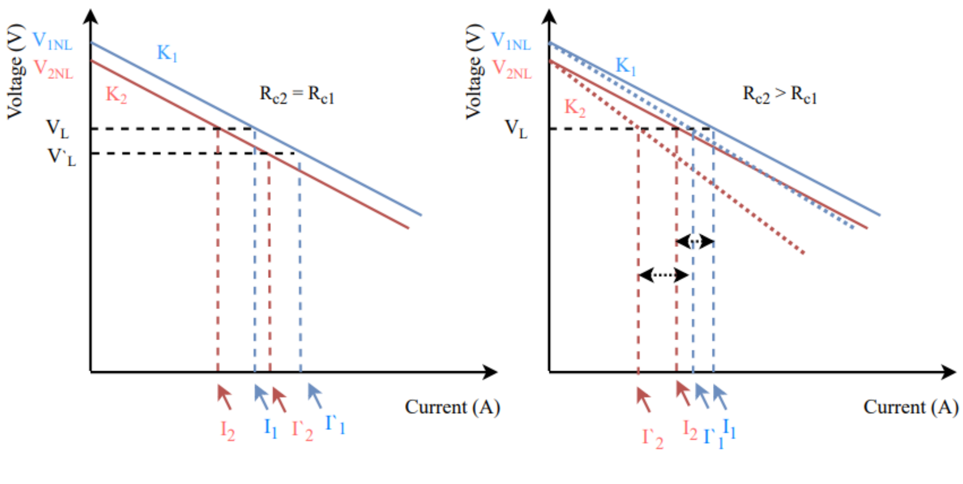


(a) (b)

Fig. 54 Load regulation characteristics of parallel-connected converters (a) Connected to the load through equal cable resistance (b) Connected to the load through different cable resistances

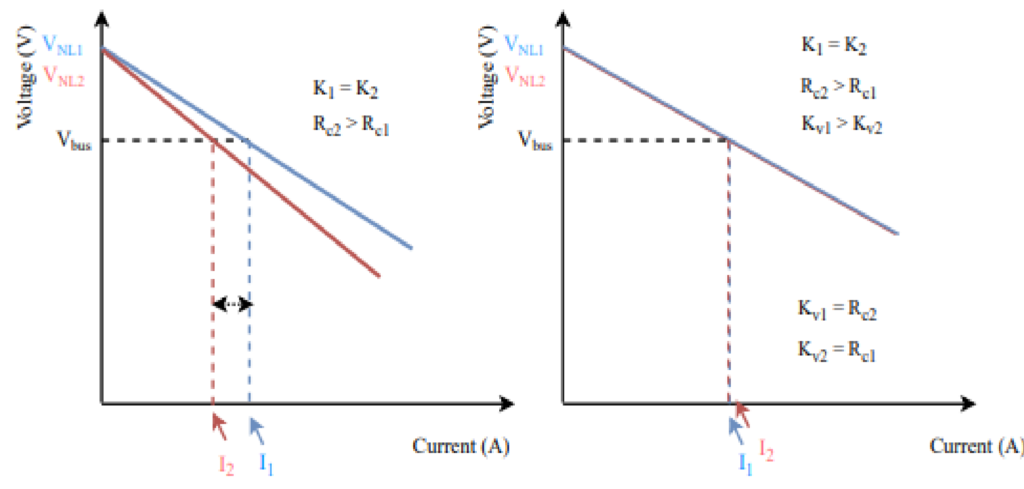


(a) (b)

Fig. 55 Implementing virtual droop gain with the load regulation characteristics of the droop method for two converters

MEMORIAL

# IMPROVED DROOP CONTROL METHOD

- **adaptive voltage control gain (AVCG)**

$$R_L = {}^{V_L}/_{I_L} \qquad (24)$$

$$I_1 = \frac{{}^{V_{NL1}}/_{R_L} - ({}^{V_{NL2}}/_{R_L{}^2}) * (K_2 + R_{c2} + R_L)}{1 - ({}^{1}/_{R_L{}^2}) * (K_1 + R_{c1} + R_L) * (K_2 + R_{c2} + R_L)} \qquad (25)$$

$$I_2 = \frac{{}^{V_{NL1}}/_{R_L} - ({}^{V_{NL1}}/_{R_L{}^2}) * (K_1 + R_{c1} + R_L)}{1 - ({}^{1}/_{R_L{}^2}) * (K_1 + R_{c1} + R_L) * (K_2 + R_{c2} + R_L)} \qquad (26)$$

The estimated voltage at the PCC (common DC bus) can be obtained

$$V_{CC} = V_{NL1} - (R_1 + K_1) * I_1 \qquad (27)$$

$$V_{CC} = V_{NL2} - (R_2 + K_2) * I_2 \qquad (28)$$

$$AVCG = V_{CC} - V_{rated} \qquad (29)$$

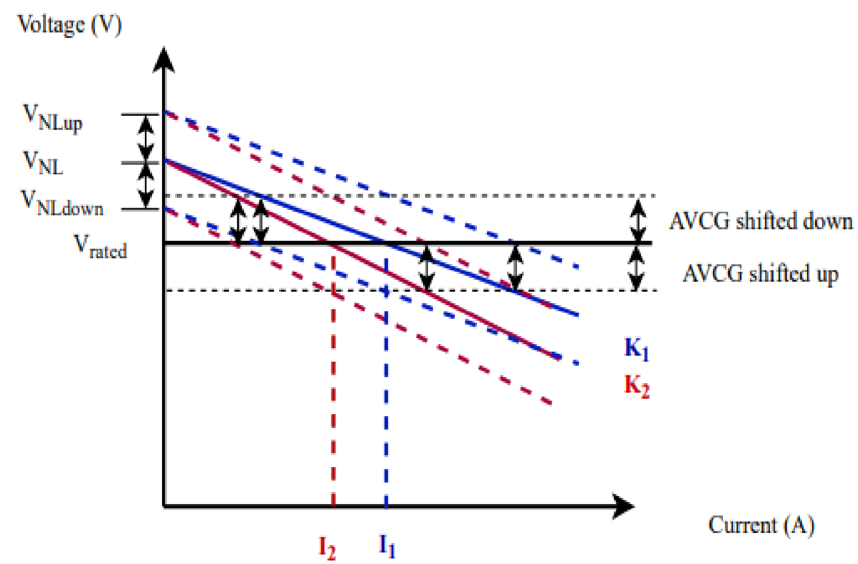


Fig. 56 load regulation characteristics of the droop method with AVCG implementation

# IMPROVED DROOP CONTROL METHOD

- **VDG and AVDG implementation with the modified Droop method**

- **10% mismatches in power stage**
- **Different cable resistance Rc1=0.2 ohm, Rc2=0.1 ohm**

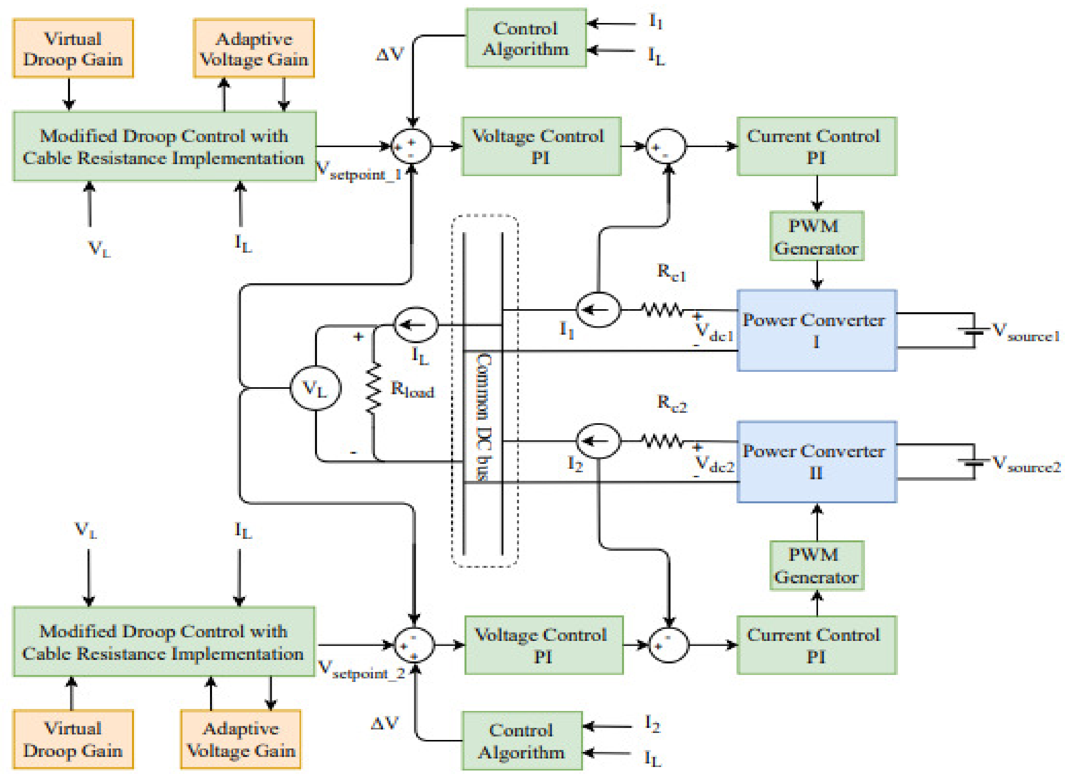


Fig. 57 Block diagram of the improved droop method

# IMPROVED DROOP CONTROL METHOD

## Simulation Results (Modified droop method Including cable resistance VS Improved droop method)

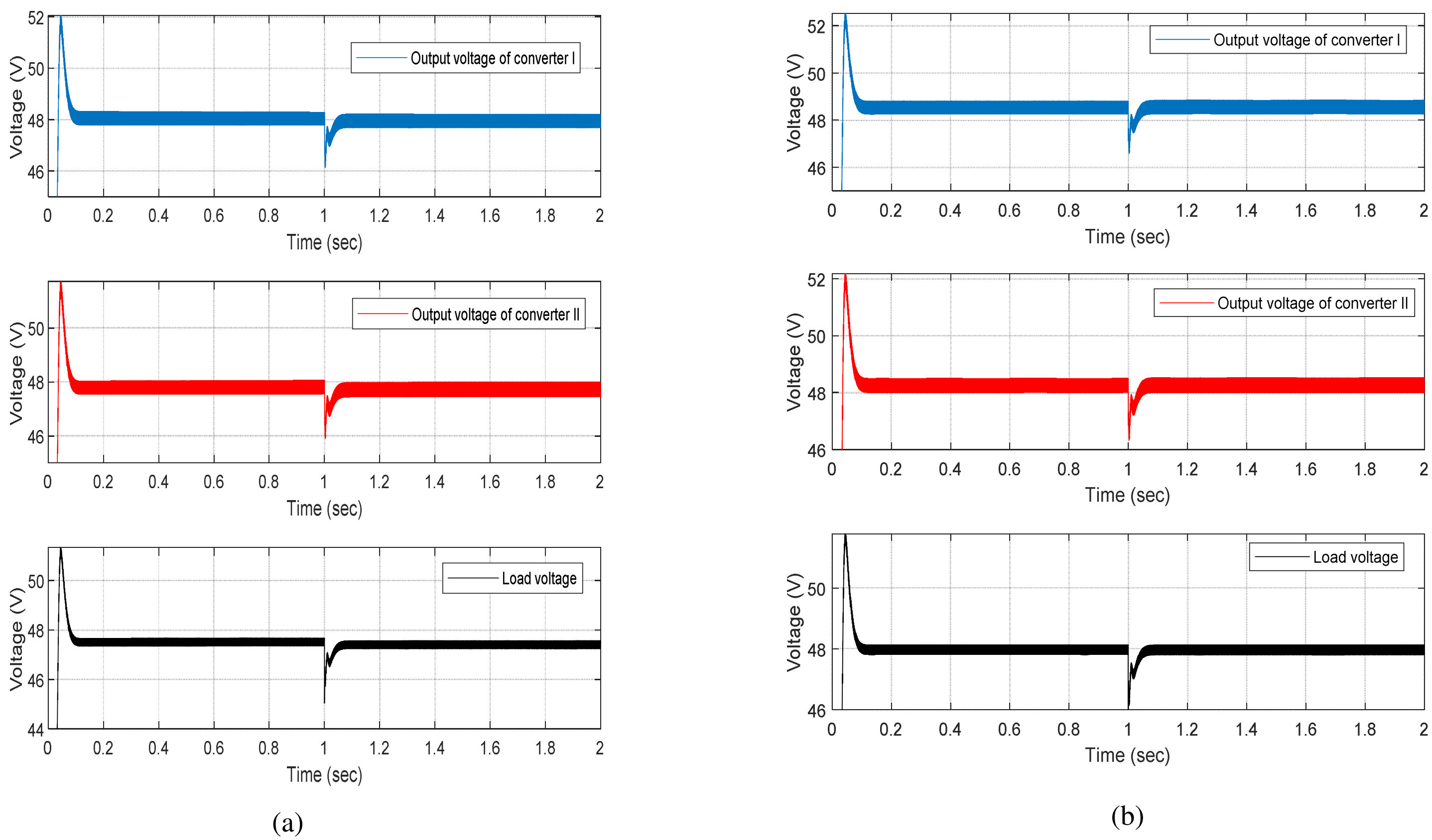


Fig. 58 Voltage response at each converter output and at the point of common coupling for a step increase in the load: (a) Output voltages for the conventional droop method and (b) Output voltages for the proposed method

# IMPROVED DROOP CONTROL METHOD

## Simulation Results (Modified droop method Including cable resistance Improved droop method)

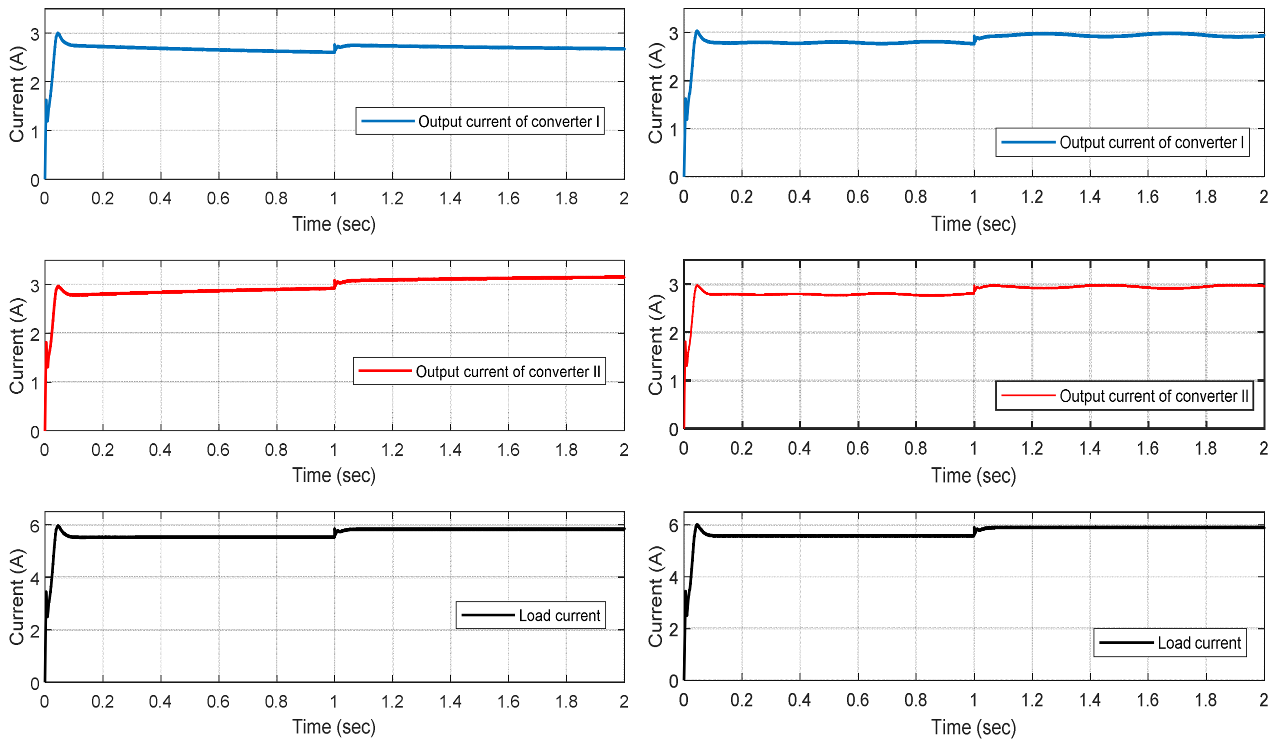


(b)

(a)

Fig. 59 Load current response for the two converters and the total load response: (a) Output currents for the conventional droop method and (b) Output currents for the proposed method

Table 5 Steady-state values for the simulation results for the voltage and current

| Method | Conventional Droop Method | | The improved Droop Method | |
|---|---|---|---|---|
| Time (s) | 0-1 | 1-2 | 0-1 | 1-2 |
| $I_1$ (A) | 2.6 | 2.68 | 2.79 | 2.94 |
| $I_2$ (A) | 2.92 | 3.14 | 2.79 | 2.94 |
| $I_L$ (A) | 5.52 | 5.82 | 5.58 | 5.88 |
| $V_{dc1}$ (V) | 48.1 | 48 | 48.5 | 48.6 |
| $V_{dc2}$ (V) | 47.8 | 47.75 | 48.29 | 48.31 |
| $V_L$ (V) | 47.5 | 47.4 | 48 | 48 |
| $\Delta I$ (%) current sharing differences | 5.8 | 7.9 | 0 | 0 |

MEMORIAL

# IMPROVED DROOP CONTROL METHOD

## Small Scale model : Simulation Results (Improved droop method)

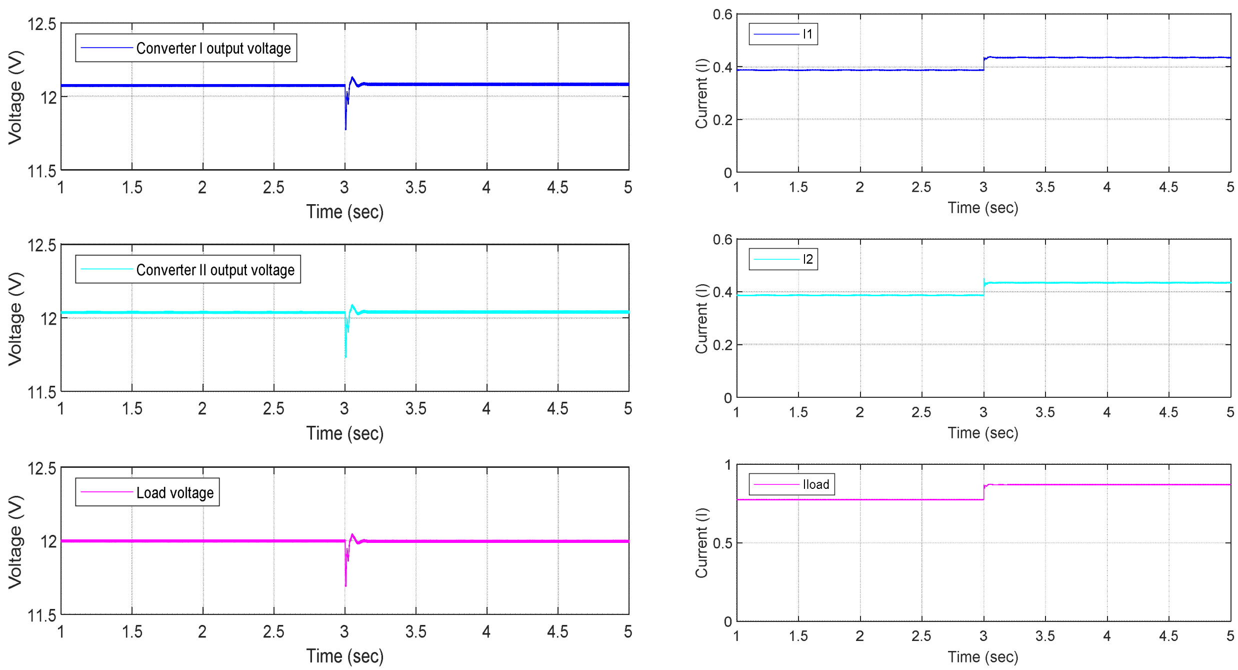


(a)

(b)

Fig. 60 Simulation results for a step increase in the load for the proposed droop method : (a) of output voltages and (b) Output currents

Table 6 Steady-state values for the simulation results for the voltage and current

| Time | 1-3 second | 3-5 second |
|---|---|---|
| $I_1$ (A) | 0.387 | 0.435 |
| $I_2$ (A) | 0.387 | 0.435 |
| $I_L$ (A) | 0.774 | 0.87 |
| $V_{dc1}$ (V) | 12.08 | 12.09 |
| $V_{dc2}$ (V) | 12.04 | 12.04 |
| $V_L$ (V) | 12 | 12 |
| $\Delta I$ (%) current sharing differences | 0 | 0 |

- Different cable resistance Rc1=0.2 ohm, Rc2=0.1 ohm

MEMORIAL

# IMPROVED DROOP CONTROL METHOD

## Small Scale model : Experimental Validation (Improved droop method)

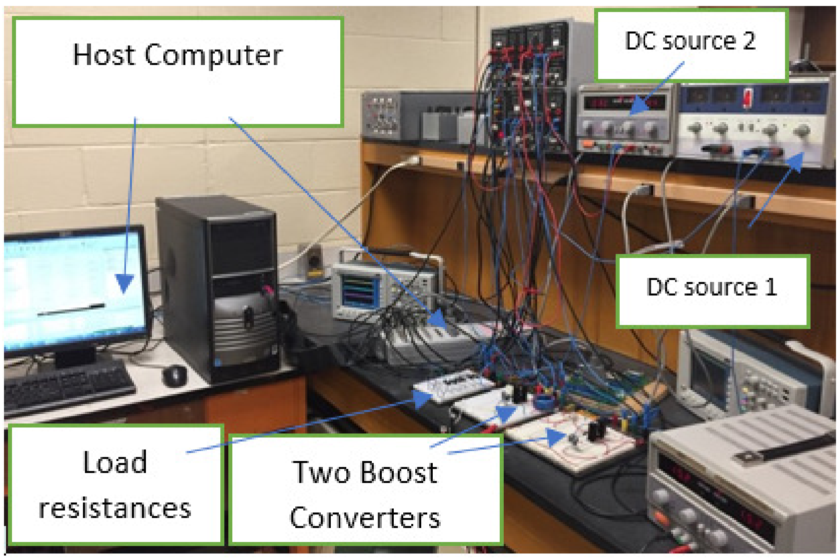


Fig. 61 Prototype parallel-connected DC boost converters system

Table 7 Parameter of boost converters

| Parameters | DC-DC Boost Converter I | DC-DC Boost Converter II |
|---|---|---|
| Switching frequency ***f*** | 25 KHz | 25 KHz |
| Inductance ***L*** | 9.136 mH | 10.20 mH |
| Capacitance ***C*** | 452 µF | 430 µF |
| Voltage V | 6-12 V | 6-12 V |

# IMPROVED DROOP CONTROL METHOD

## Small Scale model : Experimental Validation (Improved droop method)

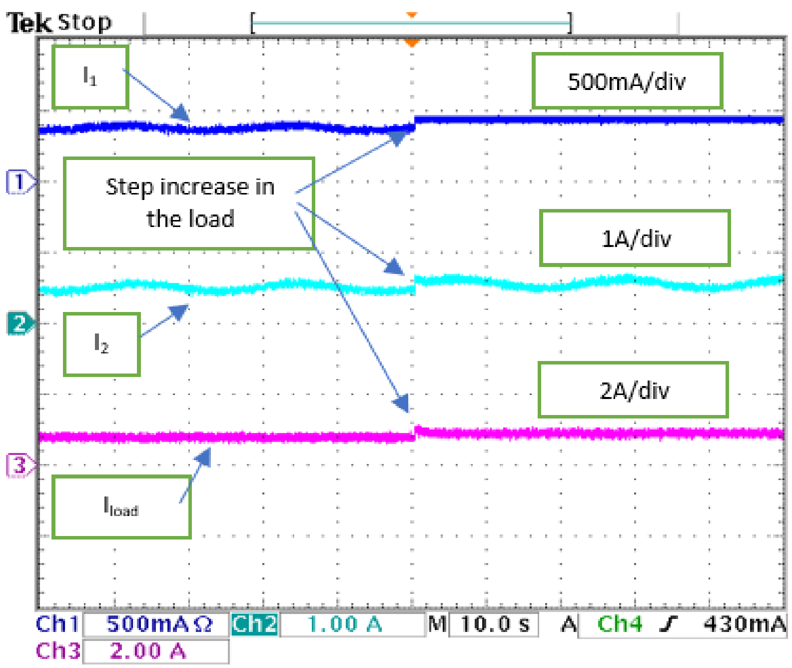


Fig. 62 Experimental results of load current sharing accuracy for a step increase in the load current

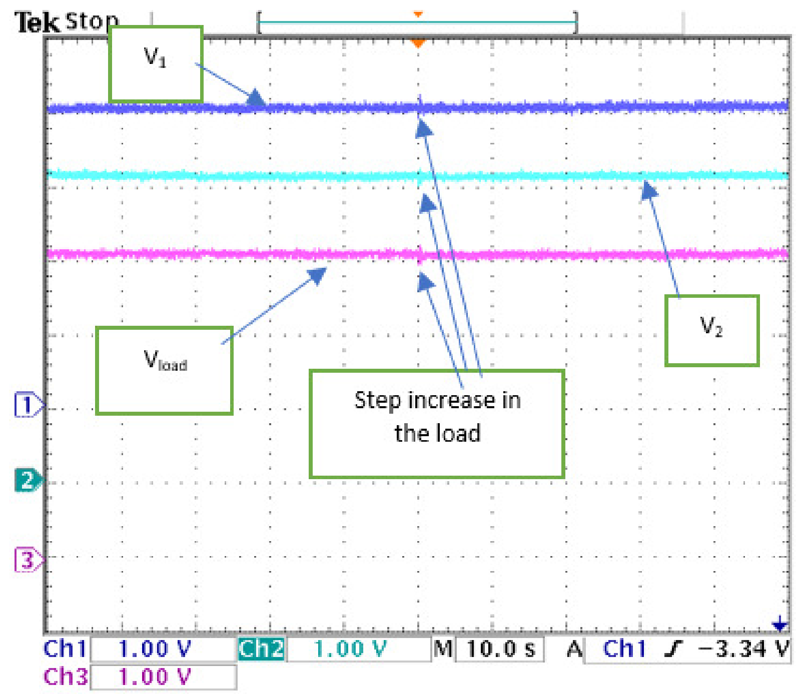


Fig 63 Experimental results of the output voltage of each converter and the voltage at the common DC bus for step change in the load current

# IMPROVED DROOP CONTROL METHOD

## Small Scale model : Experimental Validation (Improved droop method)

Table.8 Steady-state values for experimental results

| Load resistance | 15.5Ω | 13.8Ω |
|---|---|---|
| $I_1$ (A) | 0.388 | 0.436 |
| $I_2$ (A) | 0.388 | 0.436 |
| $I_L$ (A) | 0.776 | 0.872 |
| $V_{dc1}$ (V) | 12.11 | 12.09 |
| $V_{dc2}$ (V) | 12.09 | 12.10 |
| $V_L$ (V) | 12 | 12 |
| $\Delta I$ (%) current sharing differences | 0 | 0 |

MEMORIAL

# DYNAMIC MODELING, SIMULATION, AND CONTROL OF A RESIDENTIAL BUILDING MICROGRID

- **Standalone DC microgrid**
- **Powered by PV system**
- **Renewable side converter**
- **PV system fluctuates according to the variation of the solar irradiation and ambient temperature (MPPT)**
- **The load side converter (Voltage and current at PCC)**

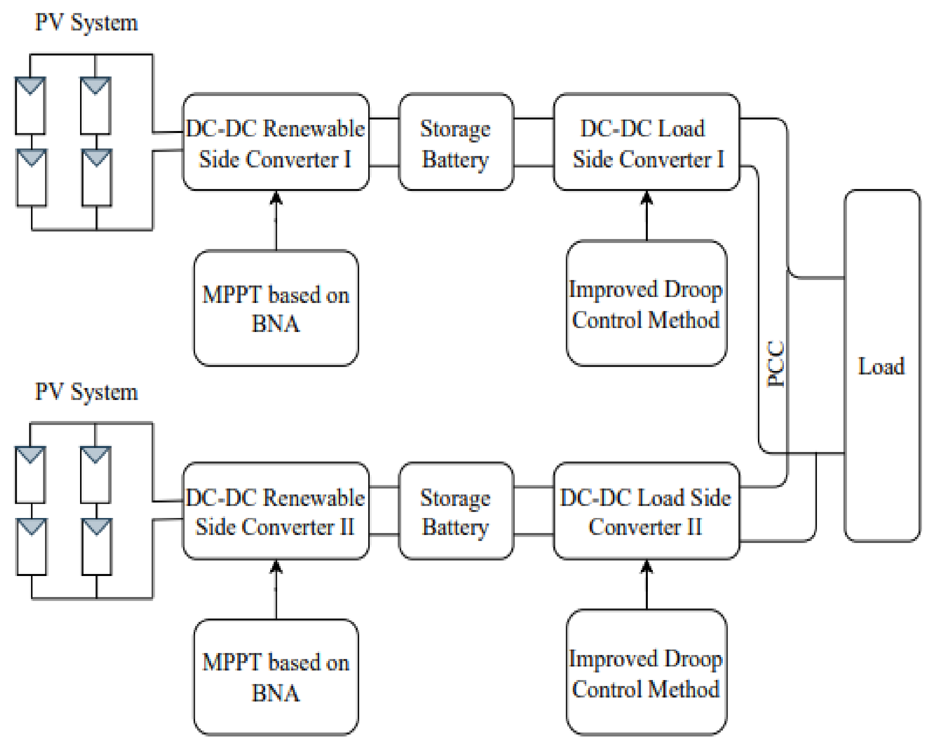


Fig. 64 Proposed standalone DC microgrid

# SIZING OF MICROGRID COMPONENTS

- **Sizing the DC microgrid for a house**
- **Location , Mesallata, Libya**
- **Area of 1000 Sqrt Ft**
- **The hourly annual electrical load based on Homer pro ( based on same weather pattern for 1000 Sqrt Ft)**
- **The solar irradiation available in the selected site**
- **The Homer Pro optimization software includes a library of solar resources worldwide, as determined by NASA's data**

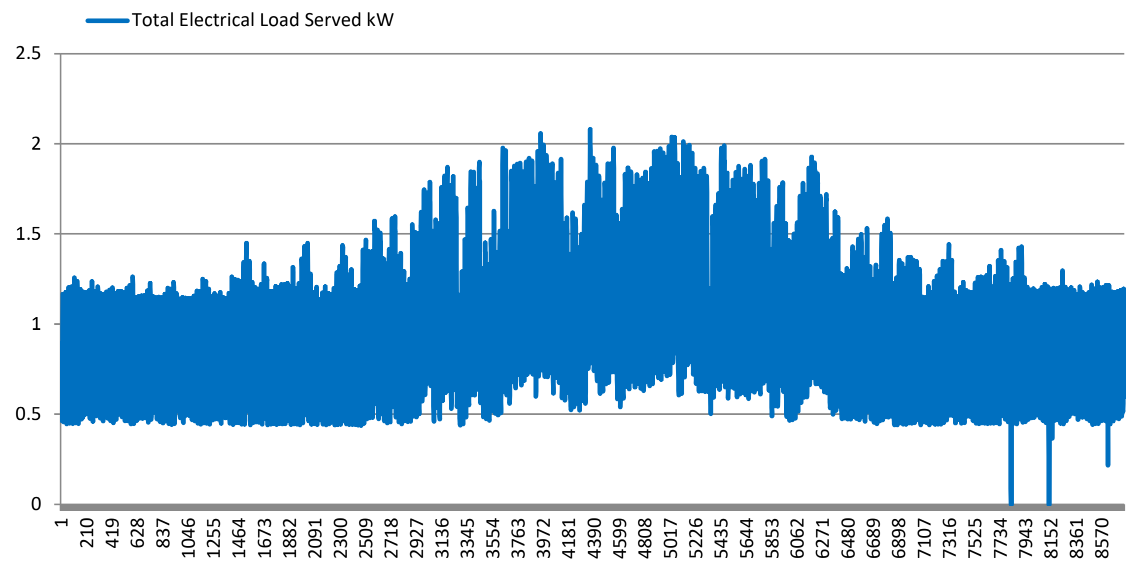


Fig. 65 Hourly load curve of 1000 $ft^2$ house in Libya

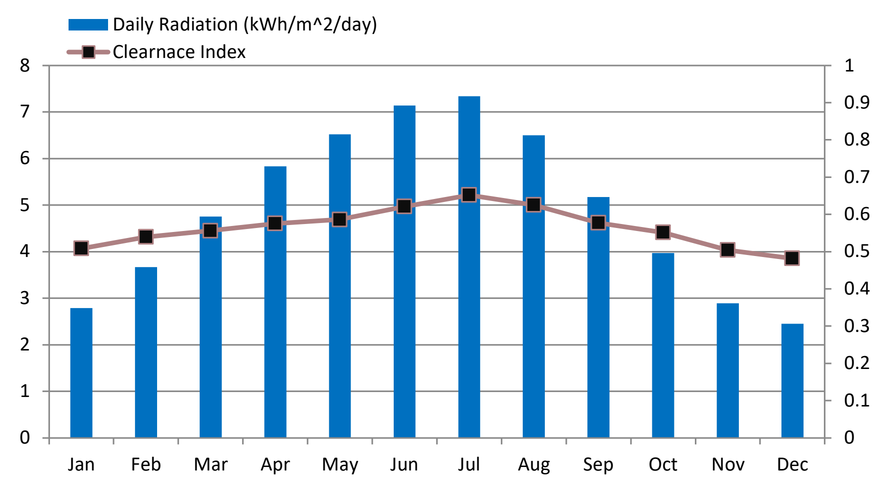


Fig. 66 Yearly solar resource in Mesallata, Libya

MEMORIAL

# SIZING OF MICROGRID COMPONENTS

- **The estimated costs for the PV system, converter, and lead-acid battery are based on the $/kW for :**

➢ **ALTE 200 Watt 24V Poly Solar Panel**

➢ **MK battery 8L16-DEKA**

➢ **Magnum Energy MS2812 converter**

- **simulate the autonomous microgrid to assess the capital, operational, cost with the size of the components**

- **the peak load and the minimum state of charge of the storage system**

Fig. 9 Input data regarding system components

| System component | Capital cost ($/kW) | Replacement Cost ($/kW) | O & M cost ($/kW/year) | Lifetime (years) | Efficiency (%) |
|---|---|---|---|---|---|
| PV system | 1095 | 1095 | 13 | 25 | 15.72 |
| Converter | 572 | 572 | 20 | 15 | 90 |
| Lead acid battery | 129 | 129 | 1.35 | 10 | 80 |

MEMORIAL

# SIZING OF MICROGRID COMPONENTS

- **Cash flow of standalone solar home system for the entire life span**
- **State of charge of the battery system 60%**
- **8 kW PV panel, 2.2 kW converter, and 70 batteries ( 420 Ah, 6 V)**

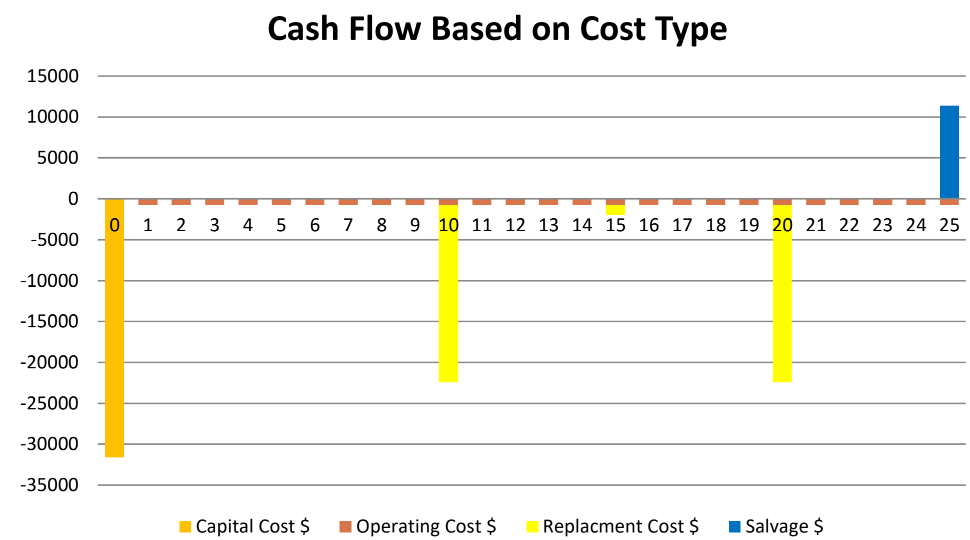


Fig. 67 Cash flow of standalone solar home system for the entire life span

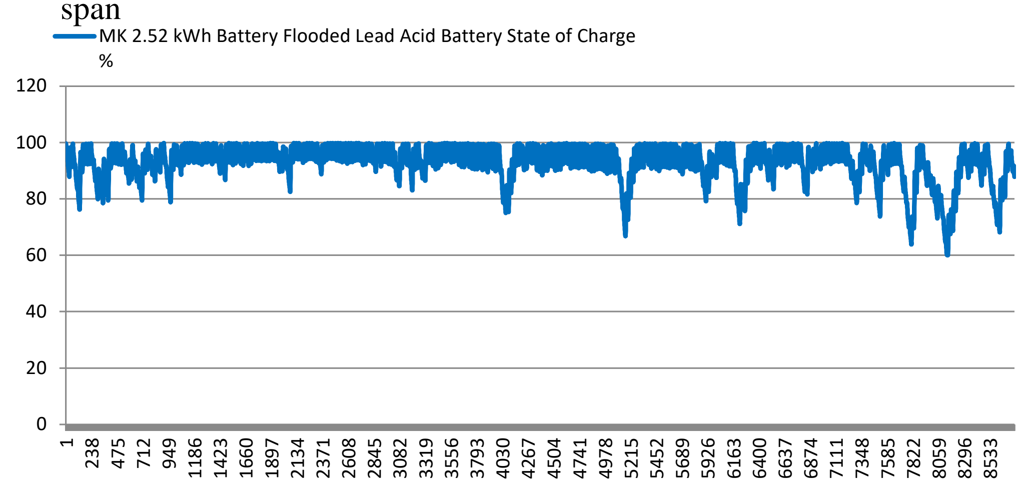


Fig. 68 State of charge of the battery storage system based on the load curve and available solar irradiation

MEMORIAL

# RENEWABLE SIDE CONVERTER (MPPT BASED ON BNA)

- **Fractional open circuit voltage FOCV and fractional short circuit current FSCC methods. (Easier to Implement – high and medium dynamic condition)**
- **Mathematical modeling of a PV in Matlab/Simulink**
- **Single diode model of The PV cell**
- **The standard test condition (STC) parameters for a KYOCERA KC200GT photovoltaic system**

TABLE 10 PARAMETERS OF the KYOCER KC200GT PV module at ( 25 C and 1000W/m^2)

| Parameters | Value |
|---|---|
| Short circuit current ( $\boldsymbol{I_{sc}}$) | 8.21 A |
| Open-Circuit Voltage ( $\boldsymbol{V_{oc}}$) | 32.9 V |
| MPP Current ( $\boldsymbol{I_{mpp}}$) | 7.61 A |
| MPP Voltage ($\boldsymbol{V_{mpp}}$) | 26.3 V |
| Temperature coefficient of $\boldsymbol{I_{sc}}$ ($\boldsymbol{k_i}$) | 0.0032 A/K |
| Temperature coefficient of $\boldsymbol{V_{oc}}$ ($\boldsymbol{k_v}$) | -0.123 V/K |
| Number of cells in series ($\boldsymbol{N_s}$) | 54 |
| Diode ideality factor ($\boldsymbol{a}$) | 1.3 |
| Series resistance ( $\boldsymbol{R_s}$) | 0.221 Ω |
| Parallel resistance ( $\boldsymbol{R_p}$) | 415.405 Ω |

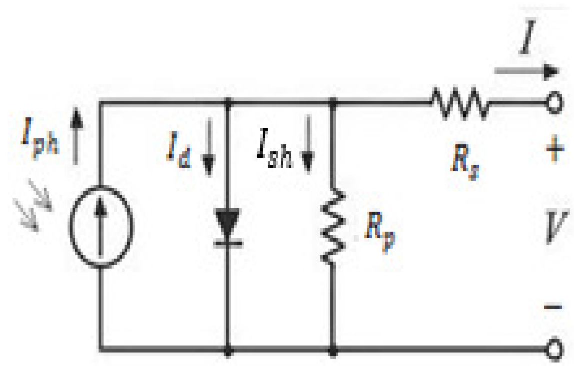


Fig. 69 Practical single diode model of the PV cell

$Pmax$ =200W

# RENEWABLE SIDE CONVERTER (MPPT BASED ON BNA)

- **P-V & I-V characteristics with different irradiance for PV module**
- **Tracking for FOCV (0.71-0.8)**
- **Tracking for FSCC (0.78-0.92)**

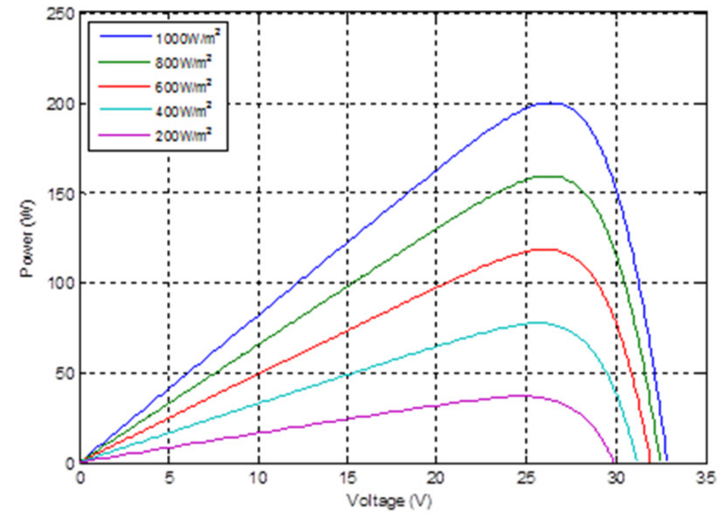


Fig. 70 P-V Characteristics with different irradiance for PV module

TABLE 11. MAXMUM POWER WITH DIFFERENT SOLAR IRRADIANCE

| Solar Irradiance $(W/m^2)$ | MPP Voltage $(V)$ | MPP Current $(A)$ | MPP Power $(W)$ |
|---|---|---|---|
| 1000 | 26.34 | 7.59 | 200 |
| 800 | 26.26 | 6.07 | 159.27 |
| 600 | 26.05 | 4.54 | 118.22 |
| 400 | 25.65 | 3.01 | 77.10 |
| 200 | 24.71 | 1.48 | 36.45 |

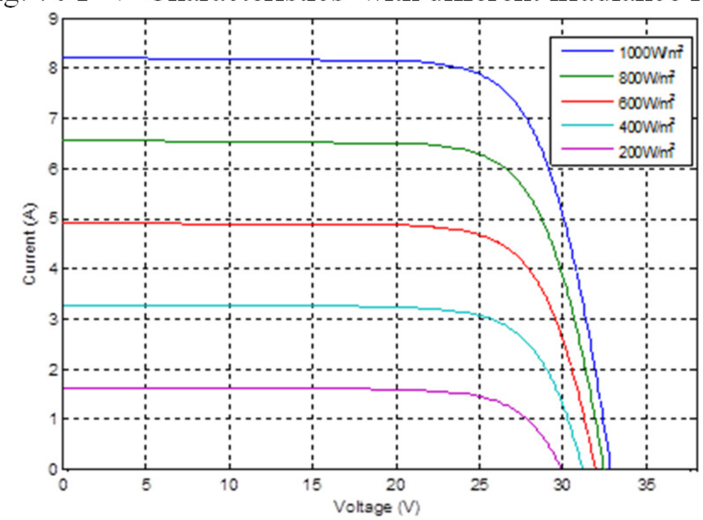


Fig. 71 I-V Characteristics with different irradiance for PV module

MEMORIAL

# RENEWABLE SIDE CONVERTER (MPPT BASED ON BNA)

- **The power as a function of the photovoltaic system output voltage**
- **The power and its derivative with respect to the output voltage at STC**

$$P = \frac{V}{1+{R_s}/{R_p}} * (I_{ph} - I_0 * (e^{\left(q*\frac{V+I*R_S}{a*N_S*K*T_{op}}\right)} - 1) - \frac{V}{R_p} \qquad (30)$$

$$P = \frac{V}{1+{R_S}/{R_p}} * (I_{ph} - I_0 * (e^{(q*\frac{V+0.9*I_{SC}*R_S}{a*N_S*K*T_{op}})} - 1) - \frac{V}{R_p}) \qquad (31)$$

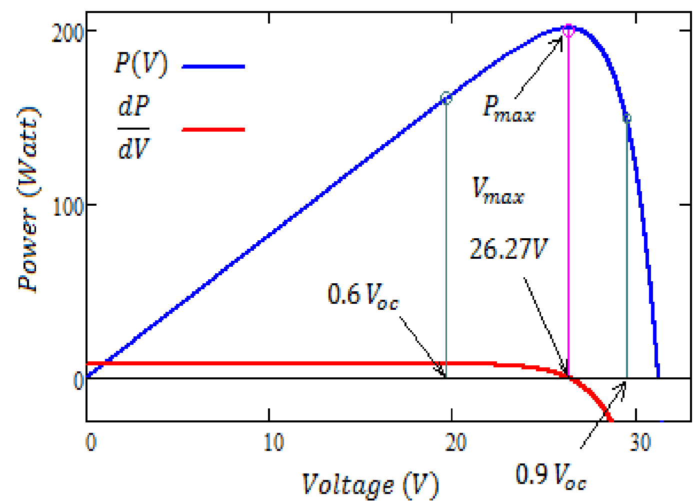


Fig. 72 P-V and dP/dV -V curves at STC

$$\frac{dP}{dV} = \frac{1}{1+{R_S}/{R_p}} * (I_{ph} - I_0 * (e^{\left(q*\frac{V+0.9*I_{SC}*R_S}{a*N_S*K*T_{op}}\right)} + V * e^{\left(q*\frac{V+0.9*I_{SC}*R_S}{a*N_S*K*T_{op}}\right)} * \frac{1}{({q}/{a*N_S*K*T_{op}})} - 1) - \frac{2*V}{R_p}) \qquad (32)$$

# RENEWABLE SIDE CONVERTER (MPPT BASED ON BNA)

- **The calculated error in voltage with different values of the irradiance**
- **Flow Chart of Bisectional Numerical Algorithm Based MPPT**

TABLE 12. The resulted Error in the Bisection Numerical Algorithm

| Irradiance $W/m^2$ | Actual MPP Voltage ($V$) | BNA MPP Voltage ($V$) | Error in the result of BNA % |
|---|---|---|---|
| 400 | 25.65 | 25.58 | 0.25% |
| 600 | 26.05 | 25.99 | 0.23% |
| 800 | 26.26 | 26.18 | 0.30% |
| 1000 | 26.34 | 26.27 | 0.28% |

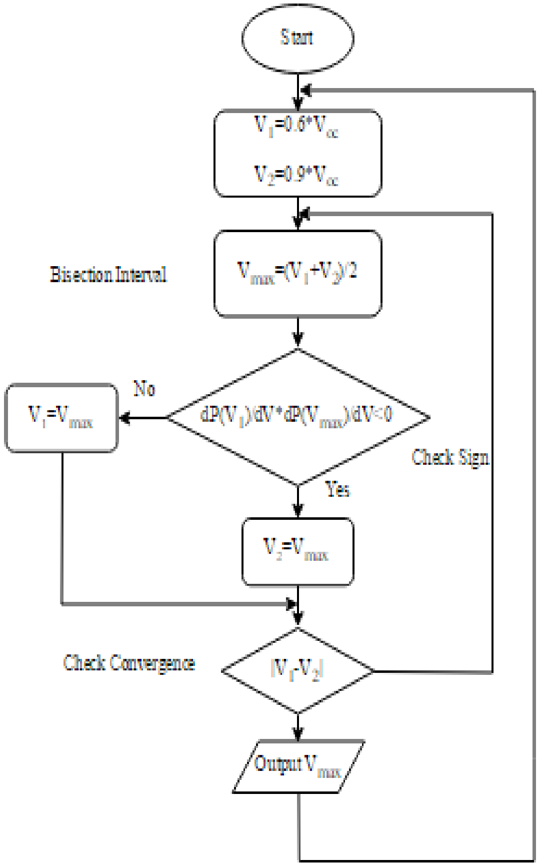


Fig. 73 Flow chart of bisectional numerical algorithm based MPPT

# RENEWABLE SIDE CONVERTER (MPPT BASED ON BNA)

- **Implementation of Bisectional Numerical Algorithm Based MPPT in MATLAB**

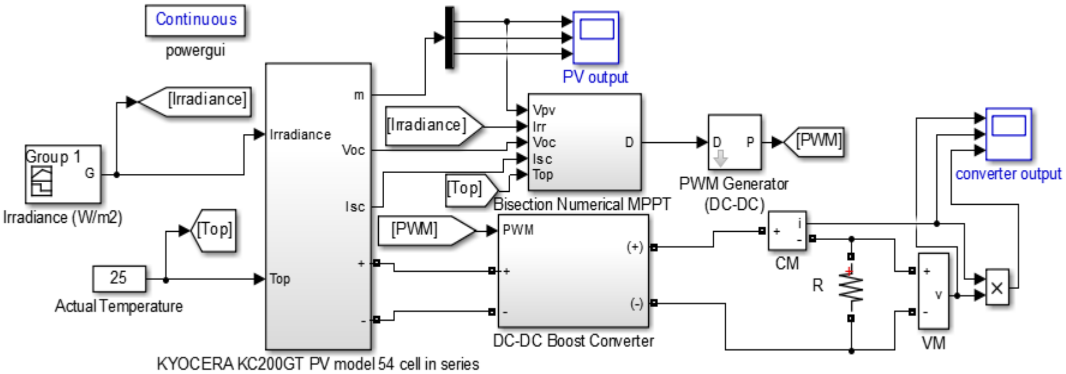


Fig. 74 Implementation of BNA Based MPPT in Matlab

TABLE 13. Tracking accuracy of the BNA method

| Irradiance / MPPT Algorithm | | Bisection numerical algorithm |
|---|---|---|
| $1000\ W/m^2$ | $P_{max}$ | 192.8 W |
| | TA % | 96.4 % |
| $800\ W/m^2$ | $P_{max}$ | 154 W |
| | TA % | 96.7 % |
| $600\ W/m^2$ | $P_{max}$ | 114.4 W |
| | TA % | 96.8 % |
| $400\ W/m^2$ | $P_{max}$ | 74.65 |
| | TA % | 96.8% |

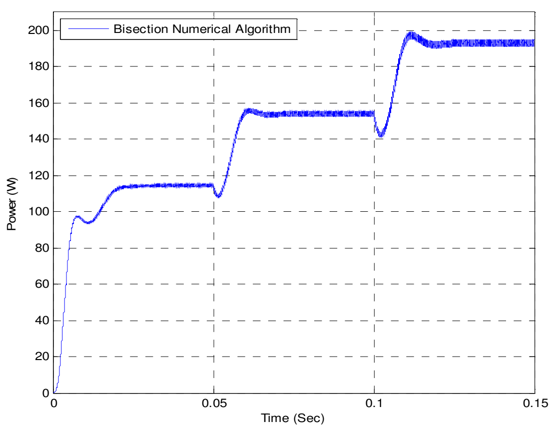


(a) Step input solar irradiance case

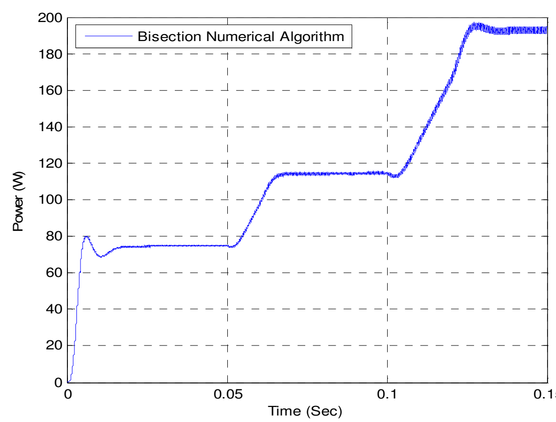


(b) Ramp input solar irradiance case

Fig. 75 Performance of the MPPT based on BNA under step and ramp input of solar irradiation

# RENEWABLE SIDE CONVERTER (MPPT BASED ON BNA)

- **Performance of Solar-PV System Connected to a Battery Storage System (BESS)**
  - **MPPT based On BNA for the DC-DC renewable side converter**
  - **8 kW PV panel, and 70 batteries ( 420 Ah, 6 V)**
  - **Two of 4 kW PV panel, 35 batteries (420A, 6V)**
  - **Solar PV of Alte 200-Watt 24V poly solar panel (Array of 10 strings of 2 panels)**
  - **Buck Converter**

TABLE 14. Electrical parameters for the Alte 200-Watt 24V poly solar panel

| | |
|---|---|
| Open-Circuit Voltage ($V_{oc}$) | 44.56V |
| Optimum Operating Voltage ($V_{mp}$) | 36.70V |
| Short-Circuit Current ($I_{sc}$) | 5.99A |
| Optimum Operating Current ($I_{mp}$) | 5.45A |
| Maximum Power at STC ($P_{max}$) | 200 W |
| Module Efficiency | 15.72% |
| Operating Temperature | -40°C to 85°C |
| Maximum System Voltage | 1000V DC |
| Power Tolerance | 0/ +5% |

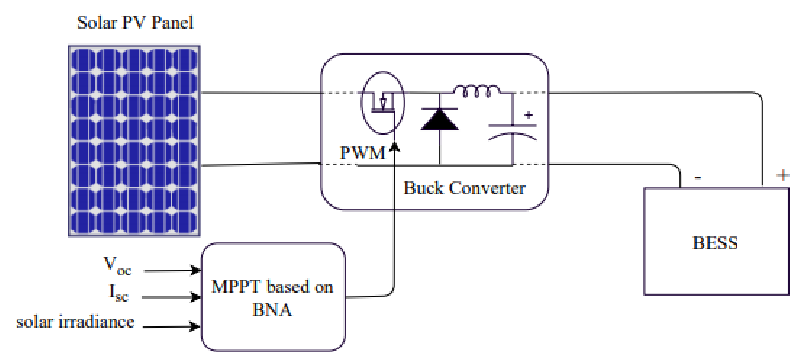


Fig. 76 Schematic diagram of the dynamic simulation model of MPPT base on BNA for solar-PV

# RENEWABLE SIDE CONVERTER (MPPT BASED ON BNA)

- **Performance of Solar-PV System Connected to a Battery Storage System (BESS**

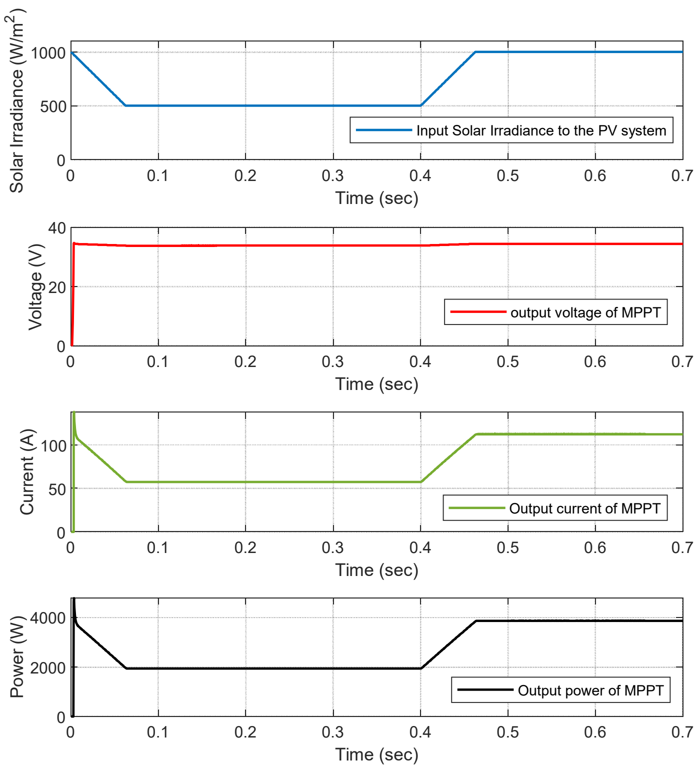


Fig. 77 Input solar irradiance, output voltage, output current, and output power of the MPPT based on the BNA for 4kW PV solar system

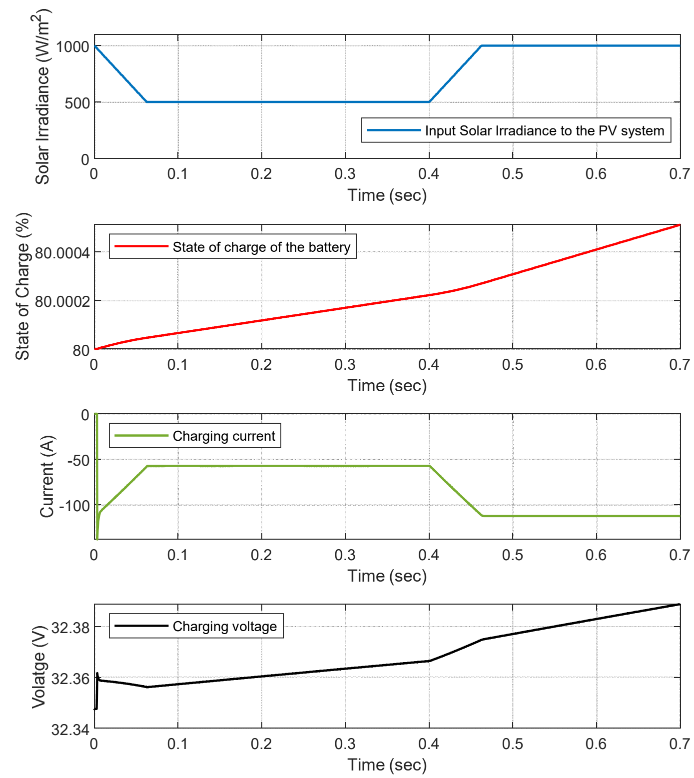


Fig. 78 Input solar irradiance, state of charge, charging current, and charging voltage of the BSSE

# PERFORMANCE OF THE SOLAR-PV ARRAY CONNECTED TO THE BESS AND THE LOAD SIDE PARALLEL-CONNECTED DC-DC CONVERTERS

- **load side parallel DC-DC boost converters is 10 % mismatch in power stage**
- **The cable resistances is selected to have values of 0.02 and 0.01 Ω (a wire gauge of 8)**
- **The initial state of charge of the BSSE is assumed to be 80%**

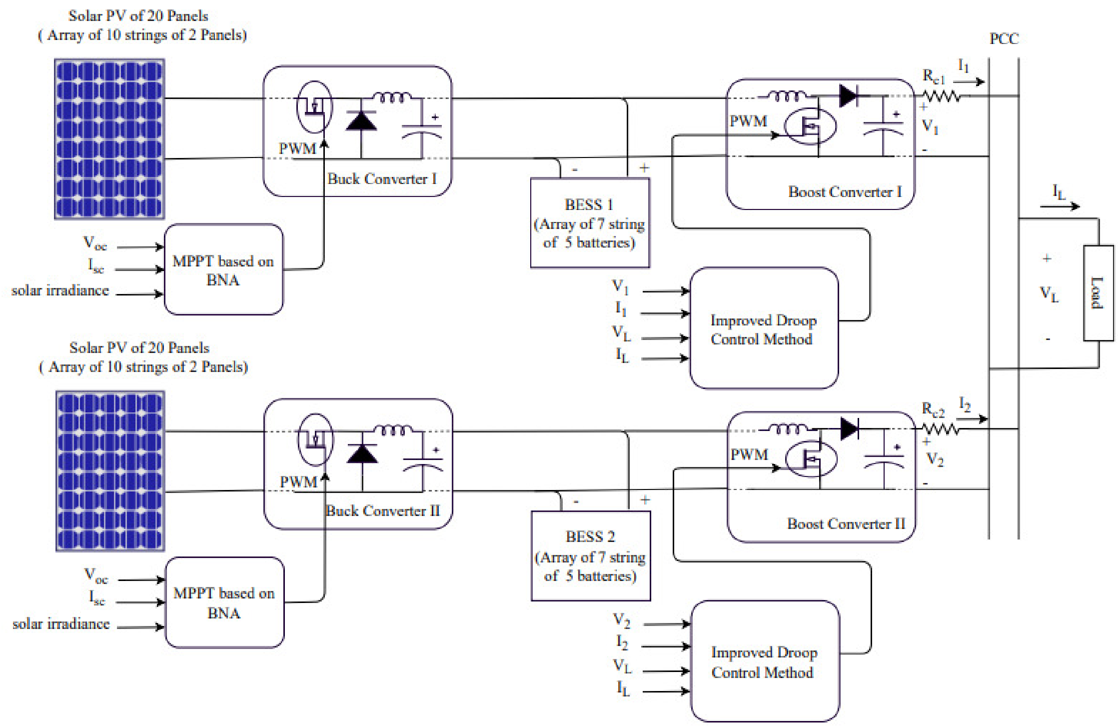


Fig. 79 schematic diagram of standalone DC microgrid

# PERFORMANCE OF THE SOLAR-PV ARRAY CONNECTED TO THE BESS AND THE LOAD SIDE PARALLEL-CONNECTED DC-DC CONVERTERS

- **load is higher than PV solar system production**
- **The PV solar system production is higher than the DC load**

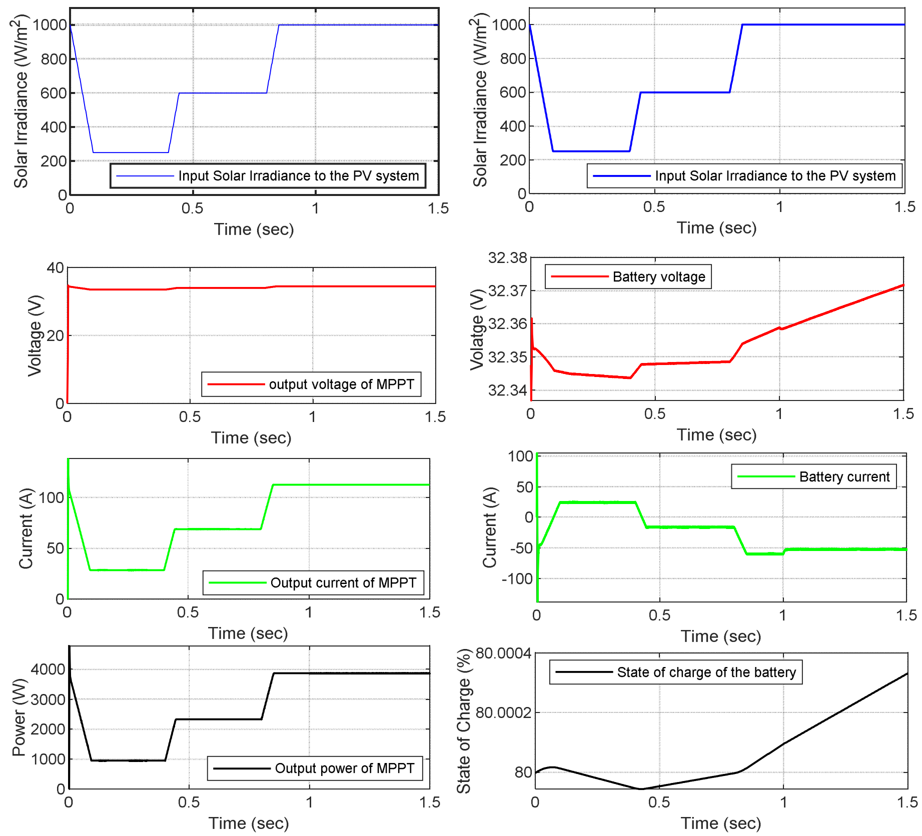


Fig. 80 Response at solar side converter (a)Input solar irradiance, output voltage, output current, and output power of the MPPT based on the BNA for 4kW PV solar system (b) Input solar irradiance of the 4 kW PV System, voltage of the battery, battery current, and the state of charge

# PERFORMANCE OF THE SOLAR-PV ARRAY CONNECTED TO THE BESS AND THE LOAD SIDE PARALLEL-CONNECTED DC-DC CONVERTERS

- **Parallel-connected Boost converters**
- **Improved droop method**
- **Load current sharing**
- **Load voltage (Voltage at the PCC)**

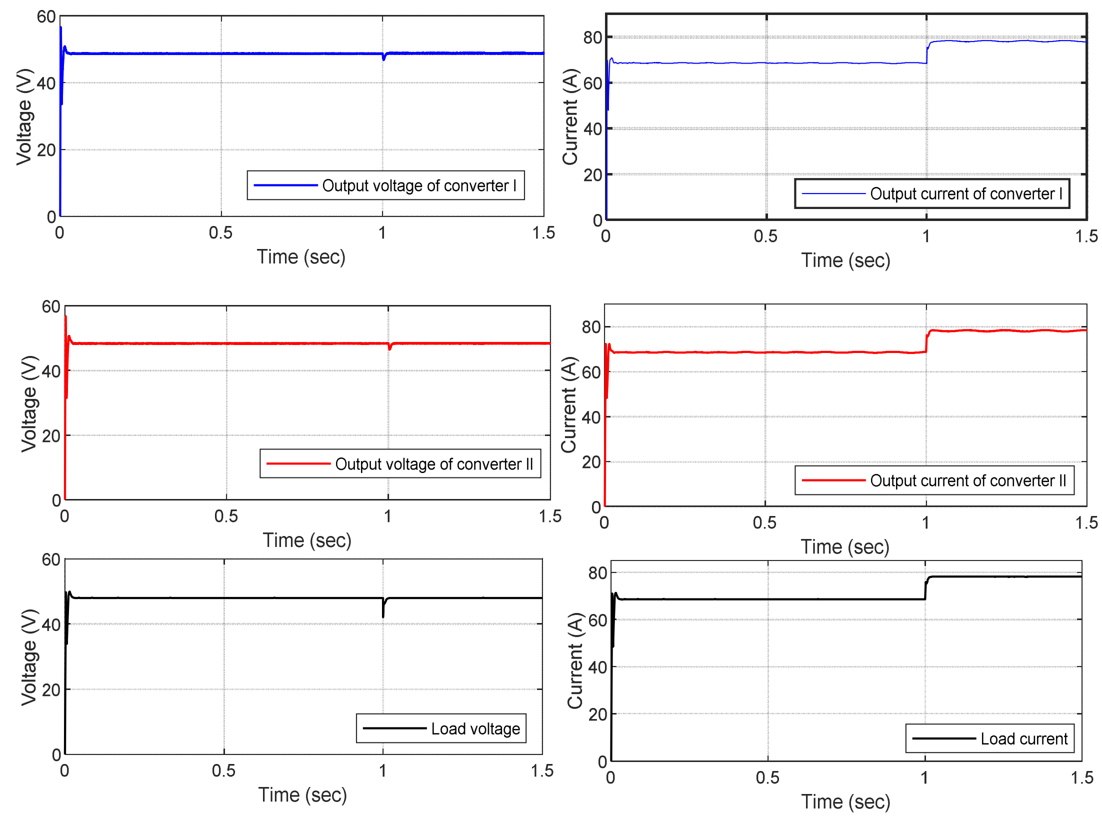


Fig. 81 Response of the parallel-connected boost converter for various load conditions (a) Output voltage of converter I and II and voltage at the common DC bus (b) Load current sharing accuracy and the total load current

# PERFORMANCE OF THE SOLAR-PV ARRAY CONNECTED TO THE BESS AND THE LOAD SIDE PARALLEL-CONNECTED DC-DC CONVERTERS WITH A PARTIAL AC LOAD

- **The same input solar irradiance of the previous case**
- **Partial AC Load**

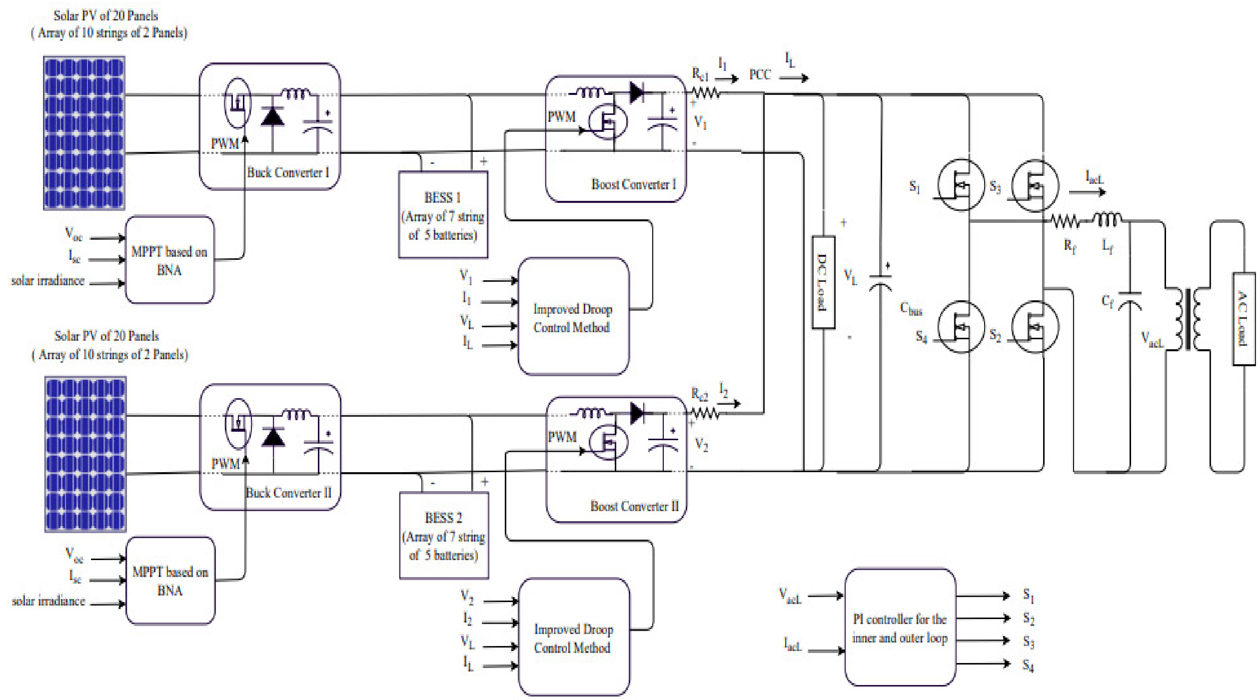


Fig. 82 Response of the parallel-connected boost converter for various load conditions (a) Output voltage of converter I and II and voltage at the common DC bus (b) Load current sharing accuracy and the total load current

# PERFORMANCE OF THE SOLAR-PV ARRAY CONNECTED TO THE BESS AND THE LOAD SIDE PARALLEL-CONNECTED DC-DC CONVERTERS WITH A PARTIAL AC LOAD

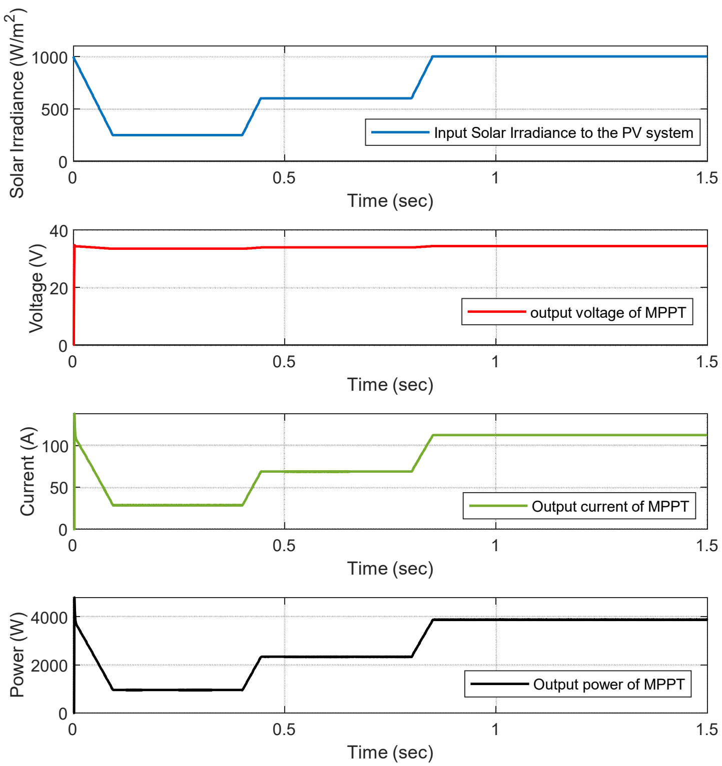


Fig. 83 Input solar irradiance, output voltage, output current, and output power of the MPPT based on the BNA for 4kW PV solar system

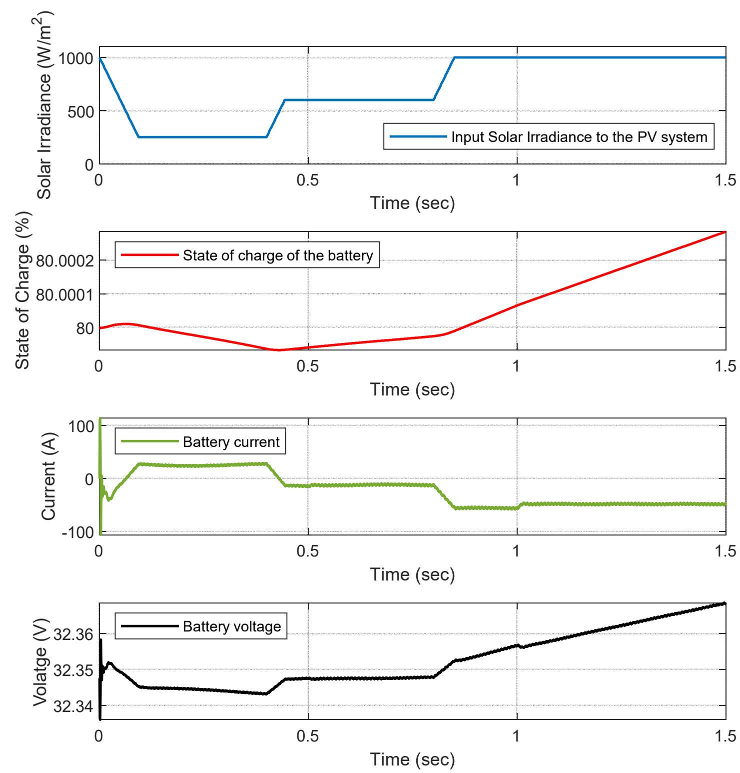


Fig. 84 input solar irradiance, and state of charge, battery voltage and current of the BSSE

MEMORIAL

# PERFORMANCE OF THE SOLAR-PV ARRAY CONNECTED TO THE BESS AND THE LOAD SIDE PARALLEL-CONNECTED DC-DC CONVERTERS WITH A PARTIAL AC LOAD

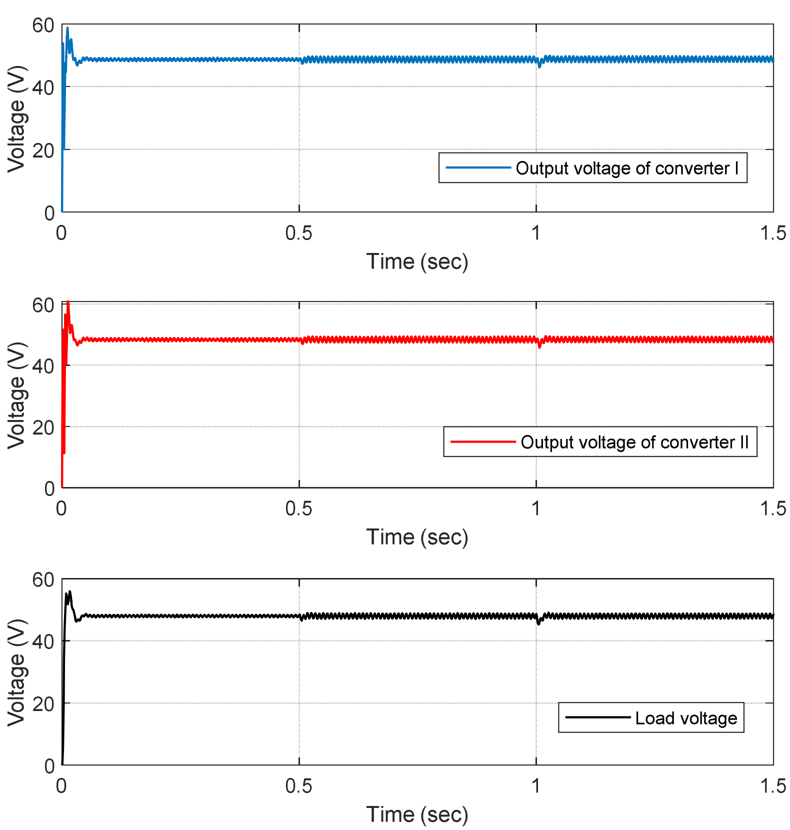


Fig. 85 Output voltage of converter I and II and the load voltage

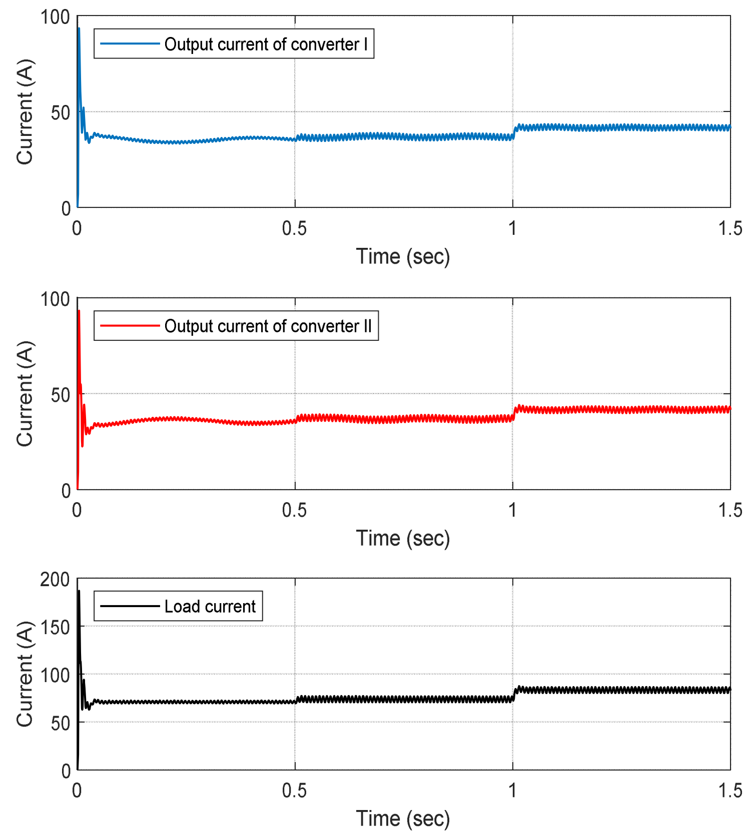


Fig. 86 Load current sharing accuracy and the total load current

- Second harmonic component

$$I_{s2} = \frac{V_o * I_o}{V_d} * \cos\left(2\omega_1 - \phi\right)$$

# CONCLUSION

**Summary:**

- A Modified droop method is proposed for estimating the set point of controlling parallel connected converters and minimizing the circulation current.
- Control algorithm is proposed for precise load current sharing and the algorithm overcomes the issue of the mismatches in converters' parameters
- Virtual droop gain is proposed for a practical solution for proper load current sharing when the differences in cable resistances is presented .
- Adaptive Voltage Control Gain Technique is proposed to improve the voltage regulation of the modified droop method.
- The proposed alternative droop strategy eliminate the need of low bandwidth communication between parallel-connected converters and provide a precise load current sharing and maintains the voltage at the PCC at the rated values.
- the BNA is proposal to overcome the tracking accuracy of the FOCV and the FSCC method.

# CONTRIBUTIONS

Published paper:

Journal papers:

1. **M.M. Shebani, T. Iqbal, and J.E. Quaicoe, "Modified Droop Method Based on Master Current Control for Parallel-Connected DC-DC Boost Converters", Journal of Electrical and Computer Engineering, Vol. 2018, p.14, 2018.**
2. **M. M. Shebani, T. Iqbal and J. E. Quaicoe, " Control Algorithm for Equal Current Sharing Between Parallel-connected Boost Converters in a DC Microgrid," , Journal of Electrical and Computer Engineering, Vol. 2020, p. 11, 2020.**
3. **M. M. Shebani, T. Iqbal and J. E. Quaicoe, " Comparison between Alternative Droop Control Strategy, Modified Droop method and Control Algorithm Technique for Parallel-connected converters,", Under revision, submitted to the journal of Electronics and Electrical Engineering, AIMS press 2020.**
4. **M. M. Shebani and T. Iqbal, "Dynamic Modeling Control and Analysis of a Solar Water Pumping System for Libya", Journal of Renewable Energy, vol. 2017, , p.13, 2017.**

Conference papers:

1. **M. M. Shebani, T. Iqbal and J. E. Quaicoe, "An Implementation of Cable Resistance in Modified Droop Control Method for Parallel-connected DC-DC Boost Converters," 2018 IEEE Electrical Power and Energy Conference (EPEC), Toronto, ON, 2018, pp. 1-6.**
2. **M. M. Shebani, T. Iqbal and J. E. Quaicoe, "Synchronous switching for parallel-connected DC-DC boost converters," 2017 IEEE Electrical Power and Energy Conference (EPEC), Saskatoon, SK, 2017, pp. 1-6.**
3. **M. M. Shebani, T. Iqbal and J. E. Quaicoe, "Comparing bisection numerical algorithm with fractional short circuit current and open circuit voltage methods for MPPT photovoltaic systems," 2016 IEEE Electrical Power and Energy Conference (EPEC), Ottawa, ON, 2016, pp. 1-5.**

# FUTURE WORK

- In the improved droop method, the VDG is determined based on the presented cable resistances in the parallel-connected converters system. The improvement in this part is associated with presenting an adaptive PI controller, which might use the PCS in order to adjust the virtual droop gain.
- The AVCG is used in the improved droop method to restore the voltage at the PCC to its rated value. This PI controller, which might be used to modify the voltage part can be enhanced by using an adaptive setpoint locally to restore the voltage at the PCC.
- For DC microgrid, balancing the state of charge for the battery energy storage systems (BESSs) with different capacities is very important. The method of improved droop control can be manipulated to balance the state of charge of BESSs with different capacities. This increases the reliability of PV-system with different capacities of the BESSs

*Thank you for Your attention …..*

- *Questions!!!!!!*